Insight into ultrasound-mediated reactive oxygen species generation by various metal-porphyrin complexes

Insight into ultrasound-mediated reactive oxygen species generation by various metal-porphyrin complexes

Francesca Giuntini[a], Federica Foglietta[b], Arianna M. Marucco[c], Adriano Troia[d], Nikolai V. Dezhkunov[e], Alessandro Pozzoli[a], Gianni Durando[d], Ivana Fenoglio[c], Loredana Serpe[b]*, Roberto Canaparo[b]

[a]School of Pharmacy and Biomolecular Sciences, Liverpool John Moores University, Liverpool L3 2AJ, UK

[b]Department of Drug Science and Technology, University of Torino, Via Pietro Giuria 13, 10125 Torino, Italy

[c]Department of Chemistry, University of Torino, Via Pietro Giuria 7, 10125 Torino, Italy

[d]National Institute of Metrological Research (INRIM), Strada delle Cacce 91, 10135 Torino, Italy

[e]Belarusian State University of Informatics and Radioelectronics (BSUIR), P. Brovka St.6, 220013, Minsk, Belarus

***Corresponding author**:

Loredana Serpe, MD PhD

Department of Drug Science and Technology, University of Torino

Via Pietro Giuria 13, 10125 Torino, Italy,

Phone: +39 011 6706235 Fax: +39 011 6706230 e-mail: loredana.serpe@unito.it

Abstract

Ultrasound is used to trigger the cytotoxicity of chemical compounds, known as sonosensitisers, in an approach called sonodynamic therapy (SDT), which is under investigation herein. The generation of reactive oxygen species (ROS) has been suggested as the main biological occurrence that leads to the cytotoxic effect. This is achieved through the synergistic action of the two components: the non-cytotoxic energy-absorbing sonosensitiser and ultrasound (US), which are both harmless *per se*. Despite some promising results, a lack of investigation into the mechanisms of US sonosensitiser-mediated ROS generation affects SDT to reach its full potential.

The aim of this work is to investigate the US-responsiveness of a variety of metal-porphyrin complexes, *i.e.*, free-base porphyrin and Fe(III), Zn(II) and Pd(II) porphyrin, by analyzing their ROS generation under US exposure and the related bio-effects. Experiments were also all carried out under light exposure as a reference.

Our results show that porphyrin ultrasound-responsiveness relies on the metal moiety present, with Zn(II) and Pd(II) porphyrin being the most efficient in generating singlet oxygen and hydroxyl radicals. ROS production efficiency is lower after ultrasound exposure than after light exposure, due to the different physico-chemical mechanisms involved in the sensitiser activation. The US porphyrin-mediated ROS generation is oxygen-dependent and the porphyrin activation by US seems more compatible with a sort of photo-activation through sonoluminescence than a radical path process through homolytic split of water. Notably, the cytotoxicity results, which are mirrored by *ex-cellulo* data, confirm that the type of ROS generation by US activation of intracellular porphyrins is pivotal for the cancer cell killing. Thus, our results may be of interest and move the technique forward in the step-by-step process towards clinical applications.

Keywords: Porphyrin; Ultrasound; Reactive oxygen species; Sonodynamic therapy; Cancer

INTRODUCTION

Sonodynamic therapy (SDT) is a proposed therapeutic approach based on the synergistic effect exerted by a combination of a suitable chemical compound (sonosensitiser) and low intensity ultrasound (US) used to kill cancer cells and microbial cells [1, 2]. The effectiveness of SDT has been demonstrated in *in vitro* and *in vivo* animal models [3-10], although the underlying mechanism of the sonosensitization is still not fully understood.

It is widely accepted that the biological effects elicited by US (in pulsed or continuous mode) are predominantly due to either a single factor or a combination of them: i) heat generation [11], ii) sonoporation [12], iii) cell membrane rupture [13] and iv) free radical generation [14]. The latter is thought to play the predominant role in SDT [15]. It has been proposed that some US-mediated biological effects rely on the occurrence of acoustic cavitation [16], a phenomenon that involves the nucleation and growth of gas-filled bubbles in a liquid milieu exposed to an appropriate US field. Specifically, bubbles in a state of stable (non-inertial) cavitation oscillate, causing streaming and mixing in the surrounding liquid/medium, whereas gas bubbles in inertial cavitation grow to near resonance size and expand to a maximum before collapsing violently [17]. In the latter case, the energy released by bubble implosion, referred to as a "sonochemical reactor", generates flashes of light known as sonoluminescence (SL) phenomenon whose UV/visible emission spectra have been investigated to determine the temperatures (from 5000 up to 15000 °K) and the pressures of bubble collapse [15, 18-21].

Acoustic cavitation is a highly complex phenomenon and, even though it is well known in a variety of scientific fields, from physics to chemistry and medicine, it is not yet completely understood. For some researchers, acoustic cavitation is thus an extreme phenomenon that is responsible for generating excessive vibration, erosion, reduced hydraulic performance and structural damages [22], while, for others, it is seen as an enormous concentration of energy with a wide range of unexplored chemical and physical consequences [23, 24]. In particular, the SL emission [25-27] has

been proposed as the pivotal trigger for the sonosensitiser-mediated generation of reactive oxygen species (ROS) in SDT [28, 29]. This hypothesis was formulated because most of the chemical compounds used in SDT are also photosensitisers [14]. It has therefore been suggested that the mechanism underlying SDT is similar to that of photodynamic therapy (PDT) [30]. Moreover, this hypothesis is consistent with the idea that sonodynamic activity might preferably take place inside cells and that singlet oxygen might play an important role in eliciting sonodynamic cytotoxicity. Even though this hypothesis has created some consensus, doubts have been expressed as to the occurrence of intracellular acoustic cavitation since it is actually unlikely to occur as such an event would lead to immediate cell destruction. However, this idea has been fostered thanks to indirect evidence, including sonodynamic cancer cell death achieved in cancer cells exposed to aminolevulinic acid [31-33], a pro-drug capable of augmenting the intracellular pool of the sonosensitiser protoporphyrin IX, and the identification of singlet oxygen by radical scavengers [29, 34]. Moreover, efficient cancer cell killing by SDT has been achieved using sensitisers of very diverse molecular structure, including porphyrins and tetrapyrroles, non-steroidal anti-inflammatory drugs, xanthenes and anticancer drugs [35, 36]. Thus, the chemical heterogeneity of the sonosensitizing species would lead to the assumption that sonosensitiser structure has no central role to play in STD and that it is simply a tool that can produce longer-lived free radicals and other highly reactive species under acoustic cavitation in order to kill cancer cells, predominantly by damaging the cell membrane.

Therefore, although it is generally agreed that the generation of free radicals is the principle cause of sonodynamic cancer cell killing, there is less consensus as to the underpinning mechanism for reactive species generation (*i.e.*, intracellular acoustic cavitation and/or sonoluminescence occurrence), the role of the sonosensitiser in the production of ROS, the kind of reactive species produced and where sonodynamic processes take places (*i.e.*, inside or outside the cells).

With this in mind, we have undertaken this study with the aim of elucidating the influence of a series of water-soluble, metal-porphyrin complexes under US exposure and light exposure, used as a reference, on ROS generation, in an attempt to evaluate the relationship between efficiency on porphyrin-mediated ROS generation and sonodynamic activity. The investigation was performed by characterizing ROS generation, by the various metal-porphyrin complexes under US or light exposure, monitoring sonoluminescence occurrence and evaluating the anticancer activity of the metal-porphyrin complexes on the colorectal cancer cell line, HT-29, under US and light exposure. Treatments were also carried out on the human dermal fibroblast cell line, HDF, to evaluate the effects on non-cancerous cells.

MATERIALS AND METHODS

Synthesis

Reagents were purchased from Sigma-Aldrich (UK), Fisher Scientific (UK) and Fluorochem (UK). Solvents were obtained from Fisher (UK). All reagents and solvents were used as supplied without further purification. Porphyrins **1**-**4** (Fig. 1) were synthesized according to methods previously reported in the literature, with some modifications [37]. NMR spectra were recorded using a Bruker Avance 300 spectrometer at 300.1 MHz (^{1}H NMR) and 75.5 MHz (^{13}C NMR) (see Supporting Materials, Fig. S1). Spectra were recorded in d_6-DMSO (Fluorochem, UK) and chemical shifts were determined relative to the residual solvent peaks at δ = 2.51 (^{1}H NMR) and δ = 39.6 ppm (^{13}C NMR). Q-TOF-MS data were acquired in positive mode, scanning from 400 to 3000 *m/z* without auto MS/MS fragmentation. Ionisation was achieved using an Agilent JetStream electrospray source and infused internal reference masses. Agilent 6540 Q-TOF-MS parameters were as follows, a gas temperature of 325 °C, a drying gas flow rate of 10 L/min, and a sheath gas temperature of 400 °C. UV-visible spectra were recorded on a Varian Cary 50 UV/vis spectrophotometer (wavelength accuracy: ± 0.24 nm). Fluorescence spectra (uncorrected) were recorded on a Cary Eclipse Fluorimeter.

*5,10,15,20-tetrakis(N-methylpyridinium-4-yl)porphyrin tetrachloride (**1**).* Methyl iodide (2 mL, 32.11 mmol) was added to a solution of 5,10,15,20-*tetrakis*-(4-pyridyl)porphyrin (500 mg, 0.80 mmol) in *N*-methylpyrrolidinone (100 mL). The resulting solution was stirred at 40 °C for 12 h. Reaction mixtures were then allowed to cool to room temperature and were treated with diethyl ether (300 mL). The supernatant was decanted and the precipitate was washed three more times with diethyl ether, decanting the supernatant each time. The solid was dissolved in water and the resulting solution was treated with 10% aqueous NH_4PF_6 (5 mL). The solid was recovered by centrifugation, dissolved in acetone and treated with 10% tetrabutylammonium chloride in acetone

(2 mL). The precipitate was collected by centrifugation and crystallised from methanol and diethyl ether to yield the desired compound (855 mg, 82%). The spectroscopic data were in agreement with the data reported in the literature.

General procedure for metal insertion into compound 1

*5,10,15,20-tetrakis(N-methylpyridinium-4-yl)porphyrinato iron(III) pentachloride (**2**).* The compound was obtained via the procedure described above, with the only difference being that the reaction mixture was maintained at 40 °C for 10 h. Compound **2** was obtained in 76% yield. Spectroscopic data were in agreement with data reported in the literature [37]. ESI-MS$^+$: [M-4Cl]$^{4+}$/4, 190.78

*5,10,15,20-tetrakis-(N-methylpyridinium-4-yl)porphyrinato zinc(II) tetrachloride (**3**).* A solution of **1** (208 mg, 0.25 mmol) in water (240 mL) was treated with $Zn(OAc)_2 \cdot 2H_2O$ (280 mg, 1.27 mmol) at room temperature. The mixture was stirred at room temperature until complete conversion was achieved (monitored by UV-visible spectroscopy and MS spectrometry), it was then diluted with water (80 mL) and treated with 10% aqueous NH_4PF_6 (2 mL). The solid was recovered by centrifugation, dissolved in acetone (30 mL) and treated with 10% tetrabutylammonium chloride in acetone (2 mL). The precipitate was collected by centrifugation and crystallised from methanol and diethyl ether to yield the desired compound (188 mg, 84%). Spectroscopic data were in agreement with data reported in the literature [37]. ESI-MS$^+$: [M-4Cl]$^{4+}$/4, 185.03

*5,10,15,20-tetrakis(N-methylpyridinium-4-yl)porphyrinato palladium(II) tetrachloride (**4**).* The compound was obtained via the procedure described above, with the only difference being that the reaction mixture was maintained at 40 °C for 10 h. Compound **4** was obtained in a 78% yield. Spectroscopic data were in agreement with data reported in the literature [38]. ESI-MS$^+$: [M-4Cl]$^{4+}$/4, 195.02

Electron spin resonance spectroscopy

The generation of ROS was monitored using electron spin resonance (EPR) spectroscopy (Miniscope 100 EPR spectrometer, Magnettech, Germany), associated with the spin trapping technique which itself used DMPO (5,5-dimethyl-1-pyrroline-N-oxide, Alexis Biochemicals, USA) and 4-oxo-TMP (2,2,6,6-tetramethyl-4-piperidone, Sigma-Aldrich) as spin-probing agents for oxygen radicals and singlet oxygen, respectively. All the other reagents were from Sigma-Aldrich. Ultrapure Milli-Q water (Millipore, Billerica, USA) was used.

Sample preparation. 600 µL of a 0.4 mM aqueous porphyrin solution were diluted in 1.9 mL of a phosphate buffered saline solution (PBS) containing either DMPO (50 mM) for hydroxyl/superoxide radical, or 4-oxo-TMP (50 mM) for singlet oxygen. The solution was either irradiated with a HgXe lamp in quartz vials for 5 min or exposed to US in a polystyrene tube for 5 min. EPR spectra were recorded, using 50 µL of the solution, immediately after treatment. In one case, the experiment was also repeated in Ar-saturated solution, *i.e.*, removing the dissolved oxygen by fluxing the solution with Ar in a controlled atmosphere for the duration of US exposure. The simulations of the EPR experimental signals were performed using Winsim 2002 software (National Institute of Environmental Health Science, National Institutes of Health, USA). Hyperfine splitting constants, obtained from the simulation optimization, were compared with those reported in the literature (NIESH STBD database).

Ultrasound exposure. The US field was generated using a plane wave transducer (2.54 cm diameter) in continuous wave mode at f = 1.866 MHz, connected to a power amplifier (Type AR 100A250A; Amplifier Research, Souderton, USA) and a function generator (Type 33250; Agilent, USA). A custom-built mechanical adaptor was connected to the 1 cm diameter polystyrene tube containing the solution. When filled with ultrapure water, the adaptor guarantees the high reproducibility of measurement conditions [39] and the distance from the transducer to the cell tube

was set at 17 mm. US exposure was performed for 5 min under subdued light at a US power of 1.5 W/cm^2. The maximum temperature recorded in the US exposed sample was 33 °C.

Light exposure. A 500 W Hg/Xe lamp (Oriel Instruments, USA), equipped with a 400 nm cut-off filter and an IR water filter to avoid suspension overheating was used. Light irradiance in the visible region was measured using a Deltahom instrument (Italy) equipped with a detector operating in the UVA and visible/NIR ranges (400-1050 nm). An irradiance of 51.8 mW/cm^2 was measured in all experiments. Irradiation was carried out for 5 min.

Sonoluminescence measurements

In order to collect the light emitted from the bubble cloud generated by the ultrasonic transducer, the transducer was inserted into the bottom of a Plexiglas tube (diameter: internal 30 mm, external 40 mm; Techno Plastic Products, Switzerland) filled with either 30 mL of 2 µM porphyrin in aqueous solution or with aqueous solution alone (control). The tube was inserted into a dark chamber at a constant temperature of 10°C (± 1°C). The emitted light was acquired by two quartz lenses, positioned on the top of the Plexiglas tube, coupled to a multicore UV-visible optical fibre connected to a monochromator (Acton SP 300i, Princeton Instruments, USA). The spectra (200-700 nm) were recorded using an LN cooled CCD (XDX mode l, Princeton Instruments) and were acquired over 3 min at a resolution of 1 nm [40]. Since SL emission decreases as the temperature of the liquid rises (a frequently observed phenomenon in liquids exposed to high-frequency US), we measured the temperature of the solution after each SL acquisition. The maximum temperature measured by means of a needle thermocouple, was 35 °C, which is consistent with the experimental conditions for cell treatment. Since in the raw spectra a low signal of SL has been reported, to improve the signal to noise ratio (S/N) of SL were also carried out experiments fluxing the solution with Ar in air atmosphere [41] for the duration of US exposure, *i.e.*, 5 min US.

Cell proliferation assay

The human colorectal cancer cell line, HT-29 (Interlab Cell Line Collection, Italy), was cultured in McCoy's 5A medium (Sigma-Aldrich) and the human dermal fibroblast cell line, HDF (ECACC, Salisbury, UK), was cultured in DMEM (Sigma Aldrich). All media were supplemented with 10% FBS (Lonza, Belgium), 2 mM L-glutamine, 100 UI/mL penicillin and 100 µg/mL streptomycin (Sigma-Aldrich) and maintained in a dark incubator (Thermo Fisher Scientific, USA) with a humidified atmosphere of 5% CO_2 air at 37 °C. At 85% confluence, cells were harvested with 0.05% trypsin-0.02% EDTA solution (Sigma-Aldrich) and suspended once again in culture medium and seeded at the appropriate cell concentration for the experiment.

In the exponential growth phase, cells were pre-incubated in the dark for 24 h with porphyrins. The cells were then normalized to 5×10^5 cells in a polystyrene tube filled with phosphate buffered saline (PBS), at pH 7.4, for sonodynamic and photodynamic treatment.

The *in vitro* sonodynamic experiment was performed under a dim light and the temperature of the medium was controlled to avoid hyperthermia during the experiment.

After treatment, 2.5 x 10^3 cells were seeded in 100 µL of culture medium in replicates (n=8) in 96-well culture plates. 10 µL of WST-1 solution (Roche Applied Science, Germany) was added at 24, 48, and 72 h and the plates were incubated at 37°C in 5% CO_2 for HT-29 cells 1.5 h and for HDF cells 2 h. Well absorbance was evaluated at 450 and 620 nm in a microplate reader (Asys UV340; Biochrom, UK). Cell proliferation data were expressed as a percentage of untreated cells.

Confocal microscopy

The HT-29 cellular uptake of porphyrins **1-4** was investigated by confocal microscopy to provide qualitative evidence for their intracellular localization. 2 x 10^5 HT-29 were left to attach for 24 h on glass coverslips in 24-well plates and were then incubated for 24 h with porphyrins **1**, **2** and **4** and with porphyrin **3** at 500 and 250 µM, respectively. At the end of the incubation time, slides

were fixed with 4% paraformaldehyde (Sigma-Aldrich) for 15 min and then cell nuclei were stained with TO-PRO®-3 (Thermo Fisher Scientific) for 15 min. Images were acquired using a Leica TCS SP5 AOBS confocal system (Leica Microsystems, Italy) equipped with a 405 nm diode, an Ar ion, and a 633-nm HeNe laser. Fixed cells were imaged using a HCX PL APO 40x 1.25 NA oil immersion objective at a pixel resolution of 0.094 × 0.094 µm.

***In vitro* sonodynamic and photodynamic treatments**

HT-29 cells in the exponential growth phase were incubated for 24 h with culture medium containing the porphyrins (**1**, **2** and **4** at 500 µM; **3** at 250 µM) in a dark incubator. The porphyrin concentration for SDT and PDT treatments was chosen to be the highest non-cytotoxic concentration obtained from the cell proliferation curves which were carried out 24 h after incubation with varying concentrations of porphyrin (125, 250, 500 and 1000 µM, see Supporting Materials, Fig. S6). Moreover, to investigate the porphyrin-dose dependency of the sonodynamic cytotoxicity, treatments at porphyrins increasing concentrations were also carried out (see Supporting Materials, Figure S6). After sonodynamic or photodynamic treatment, 2.5 x 10^3 cells were plated in a 96-well culture plate and cell proliferation was evaluated, using the WST-1 assay, 24, 48 and 72 h after treatment, as previously described.

Sonodynamic treatment. After incubation, the cells were washed with PBS, trypsinized and normalized to 5.0 x 10^5 cells in 2.5 mL of PBS in polystyrene tubes for US exposure. Cells were exposed to the US using the settings described above.

Photodynamic treatment. After incubation, the cells were washed with PBS, trypsinized and normalized to 5.0 x 10^5 cells in 2.5 mL of PBS in polystyrene tubes (Techno Plastic Products) for light exposure. Each cell tube was then irradiated in a dark box using the settings described above.

ROS scavenging assay. HT-29 cells were incubated with the ROS scavenger N-acetyl-cysteine (NAC; Sigma) in order to evaluate the role of ROS in the cytotoxicity induced by US exposure of

porphyrin-incubated cells. Briefly, cells were incubated with porphyrins (**3** at 250 µM or **4** at 500 µM) for 24 h and 5.0 mM NAC was added for the last 3 h of porphyrins incubation. Cells were then trypsinized, washed with PBS and exposed to the US using the settings described above. Cell growth was assessed using a WST-1 assay after 24, 48 and 72 h.

Treatments of non-cancerous cells. HDF cells were incubated with porphyrins and exposed to US or light in order to evaluate the effects of the treatments on the cell growth. Briefly, cells were incubated with porphyrins (**3** at 250 µM or **4** at 500 µM) for 24 h, then cells were washed with PBS, trypsinized, normalized to 1.0 x 10^5 cells in 2.5 mL of PBS in polystyrene tubes and exposed to US or light using the settings described above. Cell growth was assessed using a WST-1 assay after 24, 48 and 72 h.

Flow cytometry

ROS generation and cell death were assessed using flow cytometric assays on a C6 flow cytometer (Accuri Cytometers, USA). Sonodynamic and photodynamic ROS production was measured using 2,7-dichlorofluorescein diacetate (DCF-DA, Molecular Probes, USA) as the intracellular probe for oxidative stress. DCFH-DA is a stable, non-fluorescent molecule that readily crosses the cell membrane and is hydrolysed by intracellular esterases to the non-fluorescent DCFH, which is oxidized in the presence of peroxides to highly fluorescent 2,7-dichlorofluorescein (DCF) upon oxidation by ROS. Incubation with porphyrins was carried out as described above. Cells were then incubated with 10 µM DCFH-DA for 30 min. Following DCFH-DA incubation, cells were washed with PBS, trypsinized, normalized to 5 x 10^5 cells, collected in 2.5 mL of PBS and subjected to either sonodynamic or photodynamic treatment. ROS production was assessed 1, 5, 15, 30 and 60 min after treatment. 10,000 events were considered in the analysis. ROS production was expressed as the integrated median fluorescence intensity (iMFI), which was calculated as the product of the frequency of ROS-producing cells and the median fluorescence intensity of the cells. The iMFI

ratio was calculated in order to yield the ratiometric variation in fluorescence per time point with respect to control cells (*i.e.*, untreated cells). To limit the assay artifacts, that might influence the evaluation of the real intracellular content of the ROS induced by the treatments under investigations, the ROS detection was stopped when the iMFI ratio started to decrease due to a significant increase of DCF fluorescence in control cells [42].

Cell death was evaluated using the Dead Cell Apoptosis Kit with Annexin V-Alexa Fluor® and propidium iodide (PI, Life Technologies, Italy) 24 h after treatment. Cells were detached with trypsin and washed with PBS at 1,500 rpm for 5 min and then re-suspended with 1x Annexin-binding buffer and stained with Annexin V-Alexa Fluor® and PI. Sample analyses were carried out at 488 nm excitation, in order to measure Annexin V-Alexa Fluor® and at 530 nm to measure PI. 10,000 events were considered in the analyses and any cell debris that displayed low forward light scatter and side light scatter was excluded from the analyses. The two different staining types allowed us to identify apoptotic (Annexin V-Alexa Fluor® positive) and necrotic cells (Annexin V-Alexa Fluor® and PI positive) and tell them apart from viable cells (Annexin V-Alexa Fluor® and PI negative). All analyses were performed using FCS Express software version 4 (BD Bioscience, Italy).

Transmission electron microscopy

Samples for ultrastructural evaluation were fixed in 2.5% gluteraldehyde phosphate (pH 7.3) and stored at 4 °C for 24 h. After the post-fixation process (1% osmium for 2 h followed by a quick wash out in 30% acetone), the samples were dehydrated in acetone and embedded in Spurr resin. Thin sections (0.90 µm) were obtained from each sample using a ultramicrotome, stained with toluidine blue, and ultrathin sections (70 nm) were then contrasted with uranyl acetate and lead citrate. The grids were evaluated using a Philips CM10 transmission electron microscope.

Statistical analyses

Data are shown as mean values ± standard deviation of three independent experiments. Statistical analyses were performed on Graph-Pad Prism 6.0 software (La Jolla, USA). Two-way analysis of variance and Bonferroni's test were used to calculate the threshold of significance. The statistical significance threshold was set at $p< 0.05$.

RESULTS

Identification of ROS produced by the sonodynamic or photodynamic activation of porphyrins

The generation of ROS can be monitored by electron paramagnetic resonance (EPR) spectroscopy coupled with spin trapping, a powerful technique that is able to both identify and quantify paramagnetic species [43]. Here, specific spin trapping molecules were used to monitor the generation of superoxide radicals ($O_2^{\bullet -}$), hydroxyl radicals ($HO^{\bullet}$) and singlet oxygen ($^1O_2$). The EPR signals obtained with the spin traps DMPO (panel A) and 4-oxo-TMP (panel B), following US exposure of aqueous solutions of porphyrins **1**-**4** are shown in Fig. 2. While no signal was observed in the absence of porphyrins or without US exposure (see Supporting Materials, Fig. S2), a four line signal ($a^N = a^H$ 14.4G), that corresponds to the paramagnetic adduct DMPO/$OH^{\bullet}$, was observed in the presence of all porphyrins. Porphyrin **3** gave the highest signal intensity, indicating that it has the highest hydroxyl radical generation efficiency (Fig. 2A).

In the presence of the singlet oxygen trap, 4-oxo-TMPO, a clear three picks EPR signal (a^N 15.8 G) was observed in all samples following US exposure, while a marginally more intense signal was found with porphyrin **4** (Fig. 2B). This signal is indicative of the radical TEMPONE that is formed via the reaction of singlet oxygen with the probe 4-oxo-TMP [44-46].

The same experiments were performed under light irradiation (Fig. 3) in order to verify whether the ROS obtained from US exposure are also generated by photodynamic process. All porphyrins showed comparable singlet oxygen generation efficiency (Fig. 3B). However, a different, seven-line signal, which was particularly intense with porphyrin **2**, was observed when DMPO was used (Fig. 3A). The simulation of this signal (SI) revealed two splitting constants, one (3.9 G) with two nuclei of nuclear spin 1/2 and the other (7.1 G) with a nucleus of nuclear spin 1 (Fig. S3). This pattern corresponds to a previously identified DMPO decomposition product (DMPOX) [47].

Sonoluminescence occurrence during sonodynamic activation of porphyrins

The EPR ROS identification results, led us to investigate the occurrence of SL during the US exposure of porphyrin **3** and **4**, which showed the highest US-responsiveness (Fig. 2). The typical broad band emission of SL was observed in all the solutions tested (see Supplementary Materials, Fig. S4). In order to increase the SL S/N ratio, solutions had been fluxed with Ar during US exposure and Fig. 4. shows the SL spectra collected from porphyrin **3** and **4** solutions. Notably, an additional emission around 310-340 nm, which corresponds to $OH(A^2\Sigma^+ - X^2\ \Pi_{[1/2,3/2]})$ radical emission from vibrational bands [41], was observed being the signal more evident in porphyrin **3** solution.

Cytotoxicity induced by the sonodynamic or photodynamic activation of porphyrins

All porphyrins were taken up by HT-29 cells, which principally showed cytoplasmic distribution, after 24 h incubation (Fig. 5).

Sonodynamic and photodynamic effects on HT-29 cell growth were observed for up to 72 h after treatment. Porphyrin **1** and **2** were not able to cause a significant reduction in HT-29 cell growth under US exposure (Fig. 6). On the other hand, porphyrin **3** lead to significant HT-29 cell growth decrease under US exposure, after 72 h ($p < 0.01$), whereas porphyrin **4** caused a more marked HT-29 cell growth decrease at 48 ($p < 0.05$) and 72 h ($p < 0.001$) (Fig. 6). As observed in Fig. 7, all porphyrins induced a significant reduction in cell proliferation under light irradiation, while porphyrins **3** and **4** showed marked reductions even 48 h ($p < 0.01$) after irradiation. The key role of the sensitiser in the sonodynamic process was also highlighted by the porphyrin dose-dependency of the sonodynamic effect (see Supporting Materials, Fig. S7). Moreover, a ROS scavenging assay with NAC was carried out to clarify the correlation between intracellular ROS production and the cancer cell death induced by the sonodynamic treatment. Interestingly, NAC suppressed

cytotoxicity when HT-29 cells were treated with porphyrins and US (see Supporting Materials, Fig. S8).

It is also worth to mention that no statistically significant changes in cell proliferation were observed in HDF cells incubated with porphyrins and exposed to ultrasound (see, Supporting Materials, Fig. S9), whereas HDF cells incubated with porphyrins and exposed to light showed the same cytotoxicity pattern of HT-29 cells (Fig. 7).

Cell ROS generation by the sonodynamic or photodynamic activation of porphyrins

A cytofluorimetric evaluation of ROS generation was performed in order to evaluate whether sonodynamic and photodynamic treatment was able to induce intracellular ROS production after porphyrin excitation.

When HT-29 cells underwent US exposure, differing ROS production patterns were obtained according to the porphyrin used. As shown in Fig. 8, a significant increase in ROS production over time under US exposure was only observed when HT-29 were pre-incubated with porphyrin **3** or with porphyrin **4,** with a maximum in ROS production found 30 min after treatment ($p < 0.001$). As seen in Fig. 9, light exposure induced a maximum in ROS production 30 min after treatment in HT-29 cells that had previously been incubated with all the porphyrins under consideration ($p < 0.001$). This was followed by a progressive decrease in ROS production up to 60 min after the treatment. In particular, a significant increase in ROS production was observed 1 min after cells that had previously been incubated with porphyrin **4** were exposed to light ($p < 0.01$).

Overall, it was observed that photodynamic treatment was able to induce a significant increase in ROS production with all the porphyrins under consideration, while sonodynamic treatment was only able to induce a significant increase in ROS production in cells that had previously been incubated with porphyrin **3** and porphyrin **4**. We can also underline the fact that the results obtained by cytofluorimetric ROS evaluation are in line with the effects observed in our cell growth analysis.

Evaluation of cell death via the sonodynamic or photodynamic activation of porphyrins

As the cell death type induced by photodynamic porphyrin activation is well known, it was decided that we more deeply investigate the cell death type induced by sonodynamic porphyrin activation and that we focus our investigation on porphyrin **4**, which showed the highest US-responsiveness. As reported in Table 1, cytofluorimetric cell death analyses were performed 24 h after the sonodynamic and photodynamic treatment with porphyrin **4**. Results highlight that sonodynamic treatment was able to induce apoptotic (19.9 ± 3.1% of cell population, $p < 0.01$) and necrotic cell death (19.7 ± 4.5% of cell population, $p < 0.01$), whereas photodynamic treatment mainly induced necrotic cell death (39.7 ± 2.5% of cell population, $p < 0.001$).

Furthermore, TEM analyses were performed 12 h after sonodynamic treatment with porphyrin **4** to also investigate the role of autophagy in the sonodynamic ROS-mediated cell death. As shown in Fig. 10, control cells, *i.e.*, untreated cells, were round or oval with numerous microvilli on the plasma membrane, they contained large nuclei with homogeneous chromatin and their cell organelles were regularly distributed (Fig. 10A). In cells treated with US (Fig. 10B) or porphyrin **4**, only a moderate and irregular increase in the number of organelles or lipid droplets was observed. Interestingly, cells that have been pre-incubated with porphyrin **4** and exposed to US showed an abundance of double or single membrane-enclosed vesicles in the cytoplasm. A strong increase in lipid droplets and cell organelles was also evident (Fig. 10 C and D). This evidence indicates that porphyrin **4**-mediated sonodynamic treatment causes a change in cell metabolism, while an increase in double and single membrane-enclosed vacuoles containing, what appeared to be, damaged organelles and digested materials indicating the occurrence of autophagy.

DISCUSSION

Porphyrins are excellent sensitisers for ROS production under light irradiation while evidence of their ability to behave as sonosensitisers is slowly accumulating [28, 36, 48]. The aim of this study is to shed light on ROS formation mechanism during the sonodynamic process with porphyrin compounds. We selected 5,10,15,20-tetrakis-(methylpyridinium-4-yl)porphyrin as the core photo-sonosensitiser for its water solubility and prepared three different metal complexes, namely, Fe(III), Zn(II) and Pd(II), to introduce changes in the electronic properties of the ring, which may have affected the production of ROS (efficiency and/or type of ROS produced).

The introduction of metals in the porphyrin rings can dramatically alter the spectroscopic behaviour of the chromophore [49]. In particular, metal ions affect the ability of porphyrins to undergo intersystem crossing (ISC) and/or the lifetime of the resulting excited triplets, which in turn modifies the behaviour and the efficiency of the sensitiser [50, 51]. Indeed, free-base porphyrin **1** is moderately efficient in generating singlet oxygen following irradiation with a light beam [ ]. The insertion of Zn(II) into porphyrin **3** or Pd(II) into porphyin **4** improves the efficiency of singlet oxygen generation by enhancing ISC and facilitating conversion to the excited triplet state. Pd(II) complexes, in particular, are excellent singlet oxygen generators due to their long triplet lifetime. Moreover, insertion of Fe(III) into porphyrin **2**, a reportedly poor generator of singlet oxygen, was chosen for inclusion in the library as it is known to generate oxygen radicals via one-electron redox transformations [52]. EPR analyses performed here confirmed that this variety in ROS production behaviour and efficiency, in our photodynamic experiments, actually occurred according to the differing metal ions in the porphyrins, while some interesting features were observed. Indeed, irradiation with visible light did not lead to the formation of the DMPO/$OH^{\bullet}$ adduct (Fig. 3B), in all the porphyrins investigated, according to the EPR analysis, but instead a signal that we attributed to the DMPOX species was observed. This species is formed via the decomposition of the DMPO/$O_2^{\bullet-}$ adduct, as catalysed by low oxidation state metals [47]. The detection of this species is therefore a

proof of the occurrence of one-electron redox reactions, as expected more evident in porphyrin **2**, albeit the possible generation of DMPOX from the reaction of DMPO with singlet oxygen has also been suggested [53].

Moving to the sonodynamic experiments, the porphyrin compounds showed slightly different production behaviour and efficiency after exposure to non-thermal low intensity US than after the light exposure experiments, even though, for the first time to the best of our knowledge, EPR analyses have demonstrated the generation of hydroxyl radicals and singlet oxygen (Fig. 2A-B). However, the observed DMPO/OH$^{\bullet}$ species may also results by the decomposition of the unstable adducts of DMPO with superoxide/hydroperoxyl radicals to diamagnetic species and DMPO/OH$^{\bullet}$ [54]. It is worth noting that oxygenated radicals were clearly generated by all porphyrins, being porphyrin **3** the most efficient and that singlet oxygen was produced by all the porphyrins investigated, being porphyrin **4** the most efficient. Indeed, porphyrin **3** shows the highest signal intensity for paramagnetic adduct DMPO/OH$^{\bullet}$, whereas porphyrin **4** shows a very low signal intensity for paramagnetic adduct DMPO/OH$^{\bullet}$ (Fig. 3A). Porphyrin **4** does, however, show a more intense signal for the radical TEMPONE that is formed from the reaction of singlet oxygen with the probe 4-oxo-TMP (Fig. 3B). Therefore, it seems clear that ROS production efficiency is lower in SDT than in PDT, but at least two porphyrins, porphyrin **3** and **4**, have shown ROS production behaviour and efficiency that might suggest that a sort of photo-activation may also occur in SDT. The absence of EPR oxygenated radicals after the exposure of porphyrin **3** and **4** in Ar-saturated solutions confirms molecular oxygen as the source of US porphyrin-mediated ROS generation.

Some authors have suggested a quite peculiar US phenomenon, referred to as the emission of light by a mechanical wave, *i.e.*, sonoluminescence (SL), to explain this photo-activation mechanism that underlies the production of ROS by SDT. It was therefore decided to perform experiments to investigate the occurrence of SL is our experimental set up. Specifically, SL is the light emission in the UV-visible range caused by the ionization of noble gases inside the cavitation bubbles, which

induces the formation of a plasma that in turns ionises the molecules present in the vapour phase within the bubbles or at the gas-liquid interface of the collapsing bubble [55, 56]. SL can be observed as occurring after stimulation in the ultrasonic frequency range from 20 kHz up to 3 MHz, and is influenced by variables such as acoustic pressure, frequency, liquid proprieties, temperature and specific gas content [18]. SL emission from clouds of bubbles generated by an ultrasonic transducer is called multi-bubble sonoluminescence (MBSL) [57]. MBSL was investigated in aqueous solutions and in the presence of porphyrins **3** and **4**, which proved the most active in generating ROS upon US exposure. The typical broad band SL emission was observed for all solutions tested thus confirming the occurrence of such phenomenon. In particular, in the experiments performed fluxing the solution with Ar in an air atmosphere, SL intensity was markedly more intense than in just air atmosphere but, interestingly, some intriguing features appeared. First was an emission peak around 310-340 nm, which corresponds to emission of light by hydroxyl radicals, namely OH($A^2\Sigma^+ - X^2\ \Pi_{[1/2,3/2]}$) hydroxyl radical emission, that was evident with porphyrin **3**. Even if, the generation of hydroxyl radicals during acoustic cavitation by homolytic splitting of water was described several years ago [58], this reaction should be excluded here due to the low power of the applied US. Indeed, the absence of EPR oxygenated radical in simple aqueous solution exposed to US confirms the absence of water homolytic splitting. Therefore, our US experimental set up causes SL emissions in the UV/visible range of the electromagnetic spectrum, both in aqueous solution and in the presence of porphyrins **3** and **4** with the highest hydroxyl radical emission elicited by porphyrin **3** strengthening the hypothesis that a sort of SL activation process may play a role in the sonodynamic activation of porphyrin.

We then investigated the biological effects of the same sonodynamic and photodynamic experimental setups in an *in vitro* cancer model. Before analysing the anticancer effects of the sonodynamic or photodynamic activation of our porphyrin complexes, we confirmed their uptake by HT-29 cancer cells 24 h after incubation, as shown by confocal microscopy (Fig. 5). Upon US

exposure, the biological US-responsiveness of porphyrins **1**-**4** mirrors the results of the EPR analyses, showing the significant inhibition of cancer cell proliferation, but only when porphyrin **4** and, to a lesser extent, porphyrin **3** were used as sonosenitizers. Again the biological light-responsiveness of our porphyrin mirrors the results of the EPR analysis upon light exposure, showing a strong reduction in cancer cell proliferation with all porphyrins tested just 24 h after photodynamic treatment. The pivotal role of the sensitiser in the sonodynamic process was confirmed by the porphyrin dose-dependency of the induced cytotoxicity (Fig. S7). Moreover, the sonodynamic cytotoxicity was mainly ascribable to the porphyrin-mediated ROS production (Fig. S8) as the ROS scavenger NAC prevented the HT-29 cell death.

DCF fluorescence after our sono- and photodynamic cell treatments was measured as a redox imbalance indicator, rather than a direct measure of intracellular H_2O_2, as DCFH-DA is the most widely used probe for detecting intracellular H_2O_2 and oxidative stress [59]. The DCFH-DA assay was therefore performed to provide an indirect evaluation of intracellular ROS generation upon US or light exposure of the cells that had been pre-incubated with porphyrin **1**-**4**. Upon comparing sonodynamic and photodynamic intracellular ROS production (Fig. 8 and 9), common timing was observed. Interestingly, the highest values were observed 30 min after US or light exposure, but to differing extents according to the stimulus (US or light) and the intracellular porphyrin complex (**1**-**4**) used. Again, porphyrin **3** and **4** were found to be the most US responsive of all the porphyrins tested, at generating intracellular ROS upon US exposure, whereas all porphyrins were able to efficiently increase ROS production upon light exposure. These data support the hypothesis that the possible mechanism of action for effective sonodynamic anticancer response derives from the ROS generated by the US activation of the sensitizier, such as in the well-clinically established PDT where cancer cell killing is achieved through oxidative stress. Thus sonodynamic treatment deserves to be investigated as an intriguing strategy for cancer treatment, as also reported by other authors [60-62].

Another important aspect is the fact that PDT leads to cell death through multiple pathways. Indeed, oxidative stress mediates apoptotic and/or necrotic cell death but also autophagy, which can cause the overconsumption of the cellular machinery necessary for maintaining cellular vitality when excessive. This results in type-II programmed cell death (PCD), which is better known as "autophagic cell death" (ACD). Apoptosis and autophagic cell death can occur simultaneously, while excessive autophagy can also regulate the apoptotic pathway [63, 64], underpinning the importance of autophagy and apoptosis cross-talk when ROS are among the main intracellular signal transducers sustaining cancer cell death. Moreover, antioxidant treatment prevents autophagy, suggesting that redox imbalance has a pivotal role in driving the process. It was therefore decided to investigate the cell death induced by the porphyrin with the highest US-responsiveness, *i.e.*, porphyrin **4.** The porphyrin **4** sonodynamiyc ROS-mediated process induced both necrotic and apoptotic cell death, whereas light exposure was responsible for necrotic cell death (Table 1). These data are in agreement with the ROS analyses carried out using EPR and a DCF-DA assay. In fact, the higher necrotic rate of cell death upon photodynamic treatment may be due to the higher singlet oxygen production and redox imbalance compared to sonodynamic treatment. Moreover, TEM analyses of cells under sonodynamic treatment with porphyrin **4** were performed to investigate the possible occurrence of ACD and we were able to observe cells with significantly increased numbers of autophagosomes, giving the cell the characteristic vacuolated appearance, that is peculiar to ACD. The massive ROS production achieved upon US exposure of porphyrin **4**, is therefore able to switch the autophagic defence response against oxidative stress into a lethal stimulus leading to ACD.

The data reported here stress the relevance of the sensitiser properties for a US-induced ROS generation able to achieve cancer cell death. Indeed, different patterns of ROS generation rely on the presence and type of the metal in the macrocycle, seeing as porphrin **4** is the most efficient in generating singlet oxygen and hydroxyl radicals, and cancer cell death under US exposure.

It is worth to note, that the sonodynamic treatment of the human dermal fibroblast cell line HDF, did not exert significant effects on cell proliferation suggesting as membrane properties of the cells can be crucial for the efficiency of the sonodynamic treatment differently from what observed with the photodynamic treatment (Fig. S9). Indeed, it is well known that cell structure and mechanical properties can be very different between cancer and non-cancerous cells, in particular membrane stiffness, membrane permeability and cellular adhesion [65-67]. For istance, early stage works show relathionships bewteen elastic cell properties and US bioeffects [68, 69]. This remark may be supported by an intriguing hypothesis introduced by Krasovitski and colleagues [70], in which non-thermal US induces bilayer membrane motion that could help elucidate mechanisms of US interaction with biological tissue that are currently not fully understood. In their work, the authors presented an intracellular cavitation mechanism to explain some US biological effects, from delicate and reversible bioeffects [71] to complete membrane disruption and irreversible cellular damage [72]. Moreover, in a previous work, we have shown that the cavitation zone passes through a number of stages of evolution and SL seems to develop accordingly [27]. In this scenario, it is not unreasonable to assume that the intracellular cavitation mechanism might also elicit an intracellular cavitation zone with different stages of evolution that are able to trigger our porphyrin compounds.

In conclusion, the present work demonstrates for the first time that the sonodynamic efficacy of porphyrins in cancer cell killing can vary according to the metal moiety present in the macrocycle, since it can be responsible for different patterns of ROS generation. Moreover, there is some early *ex cellulo* evidence suggesting as the porphyrin activation by US can be due to a sort of photo-activation through sonoluminescence rather than a radical path process through homolytic splitting of water.

Author contributions

L.S. and R.C. designed the study; F.G., F.F., A.M.M., A.T. and A.P. performed research; L.S. R.C. and I.F. contributed to the analysis and interpretation of data; N.V.D. and G.D. drafted the article and revised it critically; F.G., L.S. and R.C. wrote the paper.

Competing financial interests

Tha authors declare no competing financial interests

Acknowledgment

The Authors gratefully acknowledge funding from the Associazione Italiana per la Ricerca sul Cancro (AIRC, grant "MFAG 2012", MFAG-13048) and from the University of Torino (grant "Ricerca Locale 2015"). We are grateful to Prof. Maria Teresa Capucchio for carrying out TEM analyses and Dr. Vanessa Pinnelli for assistance on *in vitro* cell experiments.

References:

[1] D. Costley, C. Mc Ewan, C. Fowley, A.P. McHale, J. Atchison, N. Nomikou, J.F. Callan, Treating cancer with sonodynamic therapy: a review, Int J Hyperthermia 31(2) (2015) 107-17.

[2] L. Serpe, F. Giuntini, Sonodynamic antimicrobial chemotherapy: First steps towards a sound approach for microbe inactivation, J Photochem Photobiol B 150 (2015) 44-9.

[3] Y. Li, Q. Zhou, Z. Deng, M. Pan, X. Liu, J. Wu, F. Yan, H. Zheng, IR-780 Dye as a Sonosensitizer for Sonodynamic Therapy of Breast Tumor, Sci Rep 6 (2016) 25968.

[4] J. Cheng, X. Sun, S. Guo, W. Cao, H. Chen, Y. Jin, B. Li, Q. Li, H. Wang, Z. Wang, Q. Zhou, P. Wang, Z. Zhang, W. Cao, Y. Tian, Effects of 5-aminolevulinic acid-mediated sonodynamic therapy on macrophages, Int J Nanomedicine 8 (2013) 669-76.

[5] D.G. You, V.G. Deepagan, W. Um, S. Jeon, S. Son, H. Chang, H.I. Yoon, Y.W. Cho, M. Swierczewska, S. Lee, M.G. Pomper, I.C. Kwon, K. Kim, J.H. Park, ROS-generating TiO2 nanoparticles for non-invasive sonodynamic therapy of cancer, Sci Rep 6 (2016) 23200.

[6] C. Brazzale, R. Canaparo, L. Racca, F. Foglietta, G. Durando, R. Fantozzi, P. Caliceti, S. Salmaso, L. Serpe, Enhanced selective sonosensitizing efficacy of ultrasound-based anticancer treatment by targeted gold nanoparticles, Nanomedicine (Lond) 11(23) (2016) 3053-3070.

[7] G. Varchi, F. Foglietta, R. Canaparo, M. Ballestri, F. Arena, G. Sotgiu, A. Guerrini, C. Nanni, G. Cicoria, G. Cravotto, S. Fanti, L. Serpe, Engineered porphyrin loaded core-shell nanoparticles for selective sonodynamic anticancer treatment, Nanomedicine (Lond) 10(23) (2015) 3483-94.

[8] V.G. Deepagan, D.G. You, W. Um, H. Ko, S. Kwon, K.Y. Choi, G.R. Yi, J.Y. Lee, D.S. Lee, K. Kim, I.C. Kwon, J.H. Park, Long-Circulating Au-TiO2 Nanocomposite as a Sonosensitizer for ROS-Mediated Eradication of Cancer, Nano Lett (2016).

[9] P. Huang, X. Qian, Y. Chen, L. Yu, H. Lin, L. Wang, Y. Zhu, J. Shi, Metalloporphyrin-Encapsulated Biodegradable Nanosystems for Highly Efficient Magnetic Resonance Imaging-Guided Sonodynamic Cancer Therapy, J Am Chem Soc 139(3) (2017) 1275-1284.

[10] Y. Lv, J. Zheng, Q. Zhou, L. Jia, C. Wang, N. Liu, H. Zhao, H. Ji, B. Li, W. Cao, Antiproliferative and Apoptosis-inducing Effect of exo-Protoporphyrin IX based Sonodynamic Therapy on Human Oral Squamous Cell Carcinoma, Sci Rep 7 (2017) 40967.

[11] G. ter Haar, Heat and sound: focused ultrasound in the clinic, Int J Hyperthermia 31(3) (2015) 223-4.

[12] I. Lentacker, I. De Cock, R. Deckers, S.C. De Smedt, C.T. Moonen, Understanding ultrasound induced sonoporation: definitions and underlying mechanisms, Adv Drug Deliv Rev 72 (2014) 49-64.

[13] W.D. O'Brien, Jr., Ultrasound-biophysics mechanisms, Prog Biophys Mol Biol 93(1-3) (2007) 212-55.

[14] A.P. McHale, J.F. Callan, N. Nomikou, C. Fowley, B. Callan, Sonodynamic Therapy: Concept, Mechanism and Application to Cancer Treatment, Adv Exp Med Biol 880 (2016) 429-50.

[15] G.Y. Wan, Y. Liu, B.W. Chen, Y.Y. Liu, Y.S. Wang, N. Zhang, Recent advances of sonodynamic therapy in cancer treatment, Cancer Biol Med 13(3) (2016) 325-338.

[16] W.L. Nyborg, Biological effects of ultrasound: development of safety guidelines. Part II: general review, Ultrasound Med Biol 27(3) (2001) 301-33.

[17] T.G. Leighton, What is ultrasound?, Prog Biophys Mol Biol 93(1-3) (2007) 3-83.

[18] K.S. Suslick, D.J. Flannigan, Inside a collapsing bubble: sonoluminescence and the conditions during cavitation, Annu Rev Phys Chem 59 (2008) 659-83.

[19] M. Kohno, T. Mokudai, T. Ozawa, Y. Niwano, Free radical formation from sonolysis of water in the presence of different gases, J Clin Biochem Nutr 49(2) (2011) 96-101.

[20] Y. Matsumura, A. Iwasawa, T. Kobayashi, T. Kamachi, T. Ozawa, M. Kohno, Detection of High-frequency Ultrasound-induced Singlet Oxygen by the ESR Spin-trapping Method, Chem Lett 42(10) (2013) 1291-1293.

[21] A. Miyaji, M. Kohno, Y. Inoue, T. Baba, Hydroxyl radical generation by dissociation of water molecules during 1.65 MHz frequency ultrasound irradiation under aerobic conditions, Biochem Biophys Res Commun 483(1) (2017) 178-182.

[22] M. Dular, B. Bachert, S. B., B. Širok, Relationship between cavitation structures and cavitation damage, Wear 257(11) (2004) 8.

[23] Y.T. Didenko, K.S. Suslick, The energy efficiency of formation of photons, radicals and ions during single-bubble cavitation, Nature 418(6896) (2002) 394-7.

[24] R. Pflieger, T. Chave, M. Virot, S.I. Nikitenko, Activating molecules, ions, and solid particles with acoustic cavitation, J Vis Exp (86) (2014).

[25] L.A. Crum, Resource Paper: Sonoluminescence, J Acoust Soc Am 138(4) (2015) 2181-205.

[26] N.V. Dezhkunov, A. Francescutto, P. Ciuti, T.J. Mason, G. Iernetti, A.I. Kulak, Enhancement of sonoluminescence emission from a multibubble cavitation zone, Ultrason Sonochem 7(1) (2000) 19-24.

[27] N.V. Dezhkunov, A. Francescutto, L. Serpe, R. Canaparo, G. Cravotto, Sonoluminescence and acoustic emission spectra at different stages of cavitation zone development, Ultrason Sonochem (2017).

[28] A. Sazgarnia, A. Shanei, H. Eshghi, M. Hassanzadeh-Khayyat, H. Esmaily, M.M. Shanei, Detection of sonoluminescence signals in a gel phantom in the presence of Protoporphyrin IX conjugated to gold nanoparticles, Ultrasonics 53(1) (2013) 29-35.

[29] S. Umemura, N. Yumita, R. Nishigaki, K. Umemura, Mechanism of cell damage by ultrasound in combination with hematoporphyrin, Jpn J Cancer Res 81(9) (1990) 962-6.

[30] C. McEwan, H. Nesbitt, D. Nicholas, O.N. Kavanagh, K. McKenna, P. Loan, I.G. Jack, A.P. McHale, J.F. Callan, Comparing the efficacy of photodynamic and sonodynamic therapy in non-melanoma and melanoma skin cancer, Bioorg Med Chem 24(13) (2016) 3023-8.

[31] Y. Shimamura, D. Tamatani, S. Kuniyasu, Y. Mizuki, T. Suzuki, H. Katsura, H. Yamada, Y. Endo, T. Osaki, M. Ishizuka, T. Tanaka, N. Yamanaka, T. Kurahashi, Y. Uto, 5-Aminolevulinic Acid Enhances Ultrasound-mediated Antitumor Activity via Mitochondrial Oxidative Damage in Breast Cancer, Anticancer Res 36(7) (2016) 3607-12.

[32] Y. Li, Q. Zhou, Z. Hu, B. Yang, Q. Li, J. Wang, J. Zheng, W. Cao, 5-Aminolevulinic Acid-Based Sonodynamic Therapy Induces the Apoptosis of Osteosarcoma in Mice, PLoS One 10(7) (2015) e0132074.

[33] Z. Hu, H. Fan, G. Lv, Q. Zhou, B. Yang, J. Zheng, W. Cao, 5-Aminolevulinic acid-mediated sonodynamic therapy induces anti-tumor effects in malignant melanoma via p53-miR-34a-Sirt1 axis, J Dermatol Sci 79(2) (2015) 155-62.

[34] W. Hiraoka, H. Honda, L.B. Feril, Jr., N. Kudo, T. Kondo, Comparison between sonodynamic effect and photodynamic effect with photosensitizers on free radical formation and cell killing, Ultrason Sonochem 13(6) (2006) 535-42.

[35] I. Rosenthal, J.Z. Sostaric, P. Riesz, Sonodynamic therapy--a review of the synergistic effects of drugs and ultrasound, Ultrason Sonochem 11(6) (2004) 349-63.

[36] H. Chen, X. Zhou, Y. Gao, B. Zheng, F. Tang, J. Huang, Recent progress in development of new sonosensitizers for sonodynamic cancer therapy, Drug Discov Today 19(4) (2014) 502-9.

[37] R.F. Pasternack, E.J. Gibbs, A. Gaudemer, A. Antebi, S. Bassner, L. De Poy, D.H. Turner, A. Williams, F. Laplace, M.H. Lansard, C. Merienne, M. Perree-Fauvet, Molecular complexes of nucleosides and nucleotides with a monomeric cationic porphyrin and some of its metal derivatives, J Am Chem Soc 107(26) (1985) 8179-8186.

[38] P.G.W.P. Harriman A, Photo-oxidation of metalloporphyrins in aqueous solution, J Chem Soc Faraday Trans 1 79 (1983) 21.

[39] B. Zeqiri, C.J. Bickley, A new anechoic material for medical ultrasonic applications, Ultrasound Med Biol 26(3) (2000) 481-5.

[40] A. Troia, D. Madonna Ripa, Sonoluminescence in liquid metals, J Phys Chem C 117(11) (2013) 6.

[41] A.A. Ndiaye, R. Pflieger, B. Siboulet, J. Molina, J.F. Dufreche, S.I. Nikitenko, Nonequilibrium vibrational excitation of OH radicals generated during multibubble cavitation in water, J Phys Chem A 116(20) (2012) 4860-7.

[42] X. Wang, H. Fang, Z. Huang, W. Shang, T. Hou, A. Cheng, H. Cheng, Imaging ROS signaling in cells and animals, J Mol Med (Berl) 91(8) (2013) 917-27.

[43] S. Mrakic-Sposta, M. Gussoni, M. Montorsi, S. Porcelli, A. Vezzoli, Assessment of a standardized ROS production profile in humans by electron paramagnetic resonance, Oxid Med Cell Longev 2012 (2012) 973927.

[44] R. Konaka, E. Kasahara, W.C. Dunlap, Y. Yamamoto, K.C. Chien, M. Inoue, Irradiation of titanium dioxide generates both singlet oxygen and superoxide anion, Free Radic Biol Med 27(3-4) (1999) 294-300.

[45] I. Fenoglio, J. Ponti, E. Alloa, M. Ghiazza, I. Corazzari, R. Capomaccio, D. Rembges, S. Oliaro-Bosso, F. Rossi, Singlet oxygen plays a key role in the toxicity and DNA damage caused by nanometric TiO2 in human keratinocytes, Nanoscale 5(14) (2013) 6567-76.

[46] M. Ghiazza, E. Alloa, S. Oliaro-Bosso, F. Viola, S. Livraghi, D. Rembges, R. Capomaccio, F. Rossi, J. Ponti, I. Fenoglio, Inhibition of the ROS-mediated cytotoxicity and genotoxicity of nano-TiO2 toward human keratinocyte cells by iron doping, J Nanopart Res 16(2) (2014).

[47] E. Finkelstein, G.M. Rosen, E.J. Rauckman, Spin trapping of superoxide and hydroxyl radical: practical aspects, Arch Biochem Biophys 200(1) (1980) 1-16.

[48] Q. Liu, X. Wang, P. Wang, L. Xiao, Sonodynamic antitumor effect of protoporphyrin IX disodium salt on S180 solid tumor, Chemotherapy 53(6) (2007) 429-36.

[49] T. Ohse, S. Nagaoka, Y. Arakawa, H. Kawakami, K. Nakamura, Cell death by reactive oxygen species generated from water-soluble cationic metalloporphyrins as superoxide dismutase mimics, J Inorg Biochem 85(2-3) (2001) 201-8.

[50] A. Harriman, Luminescence of porphyrins and metalloporphyrins. Part 1. -Zinc(II), nickel(II) and manganese(II) porphyrins, J Chem Soc Faraday Trans 1 76 (1980) 8.

[51] A. Harriman, Luminescence of porphyrins and metalloporphyrins. Part 2.-Copper(II), chromium(III), manganese(III), iron(II) and iron(III) porphyrins, J Chem Soc Faraday Trans 1 77 (1981) 9.

[52] B. Meunier, Metalloporphyrins as versatile catalysts for oxidation reactions and oxidative DNA cleavag, Chem Rev 92(6) (1992) 16.

[53] R.K. Bilski P, Bilska M & Chignell CF, Oxidation of the Spin Trap 5,5-Dimethyl-1-pyrroline N-Oxide by Singlet Oxygen in Aqueous Solution, J Am Chem Soc 118(6) (1996) 9.

[54] E. Finkelstein, G.M. Rosen, E.J. Rauckman, Production of hydroxyl radical by decomposition of superoxide spin-trapped adducts, Mol Pharmacol 21(2) (1982) 262-5.

[55] N. Garcia, A.P. Levanyuk, V.V. Osipov, Nature of sonoluminescence: noble gas radiation excited by hot electrons in cold water, Phys Rev E Stat Phys Plasmas Fluids Relat Interdiscip Topics 62(2 Pt A) (2000) 2168-76.

[56] K.S. Suslick, S.J. Doktycz, E.B. Flint, On the origin of sonoluminescence and sonochemistry, Ultrasonics 28(5) (1990) 280-90.

[57] Y.T. Didenko, T.V. Gordeychuk, Multibubble sonoluminescence spectra of water which resemble single-bubble sonoluminescence, Phys Rev Lett 84(24) (2000) 5640-3.

[58] M.W. Didenko YT, Suslick KS, Temperature of Multibubble Sonoluminescence in Water, J Phys Chem A 103(50) (1999) 6.

[59] B. Kalyanaraman, V. Darley-Usmar, K.J. Davies, P.A. Dennery, H.J. Forman, M.B. Grisham, G.E. Mann, K. Moore, L.J. Roberts, 2nd, H. Ischiropoulos, Measuring reactive oxygen and nitrogen species with fluorescent probes: challenges and limitations, Free Radic Biol Med 52(1) (2012) 1-6.

[60] H. Hirschberg, S.J. Madsen, Synergistic efficacy of ultrasound, sonosensitizers and chemotherapy: a review, Ther Deliv 8(5) (2017) 331-342.

[61] M. Trendowski, The promise of sonodynamic therapy, Cancer Metastasis Rev 33(1) (2014) 143-60.

[62] A.K. Wood, C.M. Sehgal, A review of low-intensity ultrasound for cancer therapy, Ultrasound Med Biol 41(4) (2015) 905-28.

[63] G. Filomeni, D. De Zio, F. Cecconi, Oxidative stress and autophagy: the clash between damage and metabolic needs, Cell Death Differ 22(3) (2015) 377-88.

[64] V. Inguscio, E. Panzarini, L. Dini, Autophagy Contributes to the Death/Survival Balance in Cancer PhotoDynamic Therapy, Cells 1(3) (2012) 464-91.

[65] H.H. Lin, H.K. Lin, I.H. Lin, Y.W. Chiou, H.W. Chen, C.Y. Liu, H.I. Harn, W.T. Chiu, Y.K. Wang, M.R. Shen, M.J. Tang, Mechanical phenotype of cancer cells: cell softening and loss of stiffness sensing, Oncotarget 6(25) (2015) 20946-58.

[66] H. Liu, Q. Tan, W.R. Geddie, M.A. Jewett, N. Phillips, D. Ke, C.A. Simmons, Y. Sun, Biophysical characterization of bladder cancer cells with different metastatic potential, Cell Biochem Biophys 68(2) (2014) 241-6.

[67] V. Swaminathan, K. Mythreye, E.T. O'Brien, A. Berchuck, G.C. Blobe, R. Superfine, Mechanical stiffness grades metastatic potential in patient tumor cells and in cancer cell lines, Cancer Res 71(15) (2011) 5075-80.

[68] X. Chen, R.S. Leow, Y. Hu, J.M. Wan, A.C. Yu, Single-site sonoporation disrupts actin cytoskeleton organization, J R Soc Interface 11(95) (2014) 20140071.

[69] A. Geltmeier, B. Rinner, D. Bade, K. Meditz, R. Witt, U. Bicker, C. Bludszuweit-Philipp, P. Maier, Characterization of Dynamic Behaviour of MCF7 and MCF10A Cells in Ultrasonic Field Using Modal and Harmonic Analyses, PLoS One 10(8) (2015) e0134999.

[70] B. Krasovitski, V. Frenkel, S. Shoham, E. Kimmel, Intramembrane cavitation as a unifying mechanism for ultrasound-induced bioeffects, Proc Natl Acad Sci U S A 108(8) (2011) 3258-63.

[71] W.J. Tyler, Y. Tufail, M. Finsterwald, M.L. Tauchmann, E.J. Olson, C. Majestic, Remote excitation of neuronal circuits using low-intensity, low-frequency ultrasound, PLoS One 3(10) (2008) e3511.

[72] D. Dalecki, Mechanical bioeffects of ultrasound, Annu Rev Biomed Eng 6 (2004) 229-48.

Table 1 Cell death analysis 24 h after treatment

HT-29 cells	Live cells	Apoptotic cells	Necrotic cells
Untreated cells	95.2 ± 8.3	2.5 ± 0.9	2.3 ± 0.6
Light	94.9 ± 9.2	4.1 ± 1.0	0.9 ± 0.2
US	95.0 ± 7.3	3.2 ± 0.7	1.8 ± 0.5
4	95.4 ± 8.4	4.0 ± 0.6	0.6 ± 0.1
4 + Light	53.3 ± 4.5 ***	7.0 ±0.9	39.7 ± 2.5 ***
4 + US	60.4 ± 5.8 ***	19.9 ± 3.1 **	19.7 ± 4.5 **

Statistical significance *vs* untreated cells: ** $p < 0.01$, *** $p < 0.001$.

FIGURE LEGENDS

Fig. 1 Structures of porphyrins **1**-**4**

Fig. 2 Generation of hydroxyl radicals (A) and of singlet oxygen (B) by the various porphyrins (**1**-**4**) following activation with US power at 1.5 W/cm^2 for 5 min at 1.866 MHz, as detected by EPR spectroscopy. Signal intensity is proportional to the amount of reactive species generated.

Fig. 3 Generation of hydroxyl radicals (A) and of singlet oxygen (B) by the various porphyrins (**1**-**4**) following activation with light power at 51.8 mW/cm^2 for 5 min at 400-1050 nm, as detected by EPR spectroscopy. Signal intensity is proportional to the amount of reactive species generated.

Fig. 4 Sonoluminescence emission spectra of porphyrin **3** (black curve) and **4** (red curve) solutions fluxed with Ar during US exposure at 1.5 W/cm^2 for 5 min, at 1.866 MHz. The blue curve refers to multi-bubble sonoluminescence recorded in PBS solution, while the grey curve corresponds to the background of the acquiring system after 2 min of exposure. The emission around 310-340 nm (*) is quite overlapped by broad continuum emission but is still visible and correspond to OH($A^2\Sigma^+ - X^2\ \Pi_{[1/2,3/2]}$) radical emission due to vibrational bands.

Fig. 5 Representative confocal fluorescence images of HT-29 cells incubated with the various porphyrins. Cells were exposed to either 500 μM of porphyrin **1**, **2** or **4** or 250 μM of porphyrin **3** (green) for 24 h; TO-PRO®-3 (blue) was used as nuclear counterstain. Magnification: 40x. Scale bars: 15 μm.

Fig. 6 Effects of sonodynamic treatment on HT-29 cell growth. HT-29 cells were incubated for 24 h with the various porphyrins (**1**, **2** and **4** at 500 μM; **3** at 250 μM) and then exposed to US power at

1.5 W/cm^2 for 5 min at 1.866 MHz. Cell proliferation was evaluated after 24, 48 and 72 h by WST-1 assay. Statistically significant difference versus untreated cells: * $p < 0.05$, ** $p < 0.01$.

Fig. 7 Effects of photodynamic treatment on HT-29 cell growth. HT-29 cells were incubated for 24 h with the various porphyrins (**1**, **2** and **4** at 500 μM; **3** at 250 μM) and then exposed to light power at 51.8 mW/cm^2 for 5 min at 400-1050 nm. Cell proliferation was evaluated after 24, 48 and 72 h by WST-1 assay. Statistically significant difference versus untreated cells: * $p < 0.05$, ** $p < 0.01$, *** $p < 0.001$.

Fig. 8 HT-29 reactive oxygen species production after sonodynamic treatment. HT-29 cells were exposed to US (1.5 W/cm^2 for 5 min at 1.866 MHz) alone or after 24 h incubation with the various porphyrins (**1**, **2** and **4** at 500 μM; **3** at 250 μM). ROS levels were determined according to the 2',7'-dichlorofluorescein diacetate (DCF-DA) assay by flow cytometry and expressed as the integrated average fluorescence ratio (iMFI) ratio, as described in Materials and Methods. Statistically significant difference versus untreated cells (represented by a dashed lines): * $p < 0.05$, ** $p < 0.01$, *** $p < 0.001$.

Fig. 9 HT-29 reactive oxygen species production after photodynamic treatment. HT-29 cells were exposed to light (51.8 mW/cm^2 for 5 min at 400-1050 nm), alone or after cell incubation for 24 h with the various porphyrins (**1**, **2** and **4** at 500 μM; **3** at 250 μM). ROS levels were determined according to the 2',7'-dichlorofluorescein diacetate (DCF-DA) assay by flow cytometry and expressed as the integrated average fluorescence ratio (iMFI) ratio, as described in Materials and Methods. Statistically significant difference versus untreated cells (represented by a dashed lines): * $p < 0.05$, ** $p < 0.01$, *** $p < 0.001$.

Fig. 10 Representative TEM images of HT-29 after sonodynamic treatment with porphyrin **4**. Control cells, i.e., untreated cells (A, 7,500x), cells exposed to US (1.5 W/cm^2 for 5 min at 1.866 MHz) alone (B, 7,500x) and cells 12 h after sonodynamic treatment with porhyrin **4** having been pre-incubated for 24 h at 500 μM (C, 6,000x; D, 12,000x) are displayed. Vesicles that contained residual digested materials or cellular contents are indicated by arrows and lipid droplets by stars.

Fig. 1

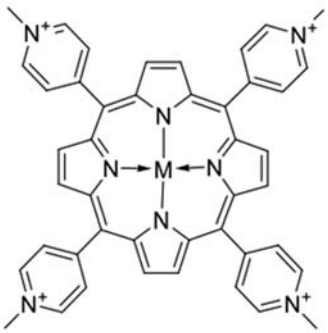

1: M = $2H^+$ **2**: M = $Fe^{3+}(Cl)$

3: M = Zn^{2+} **4**: M = Pd^{2+}

Fig. 2

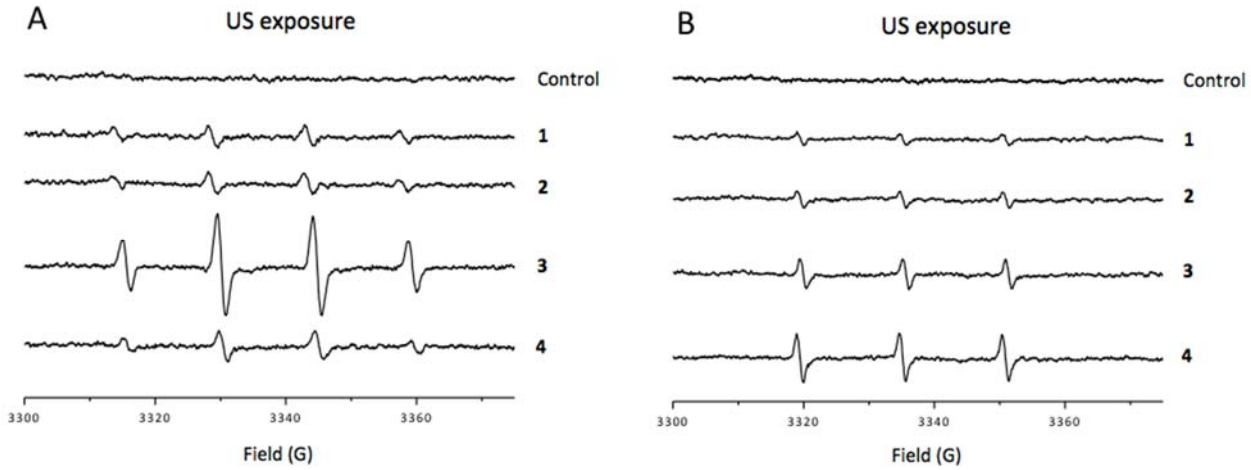
A
US exposure
Control
1
2
3
4
3300
3320
3340
3360
Field (G)
B
US exposure
Control
1
2
3
4
3300
3320
3340
3360
Field (G)

Fig. 3

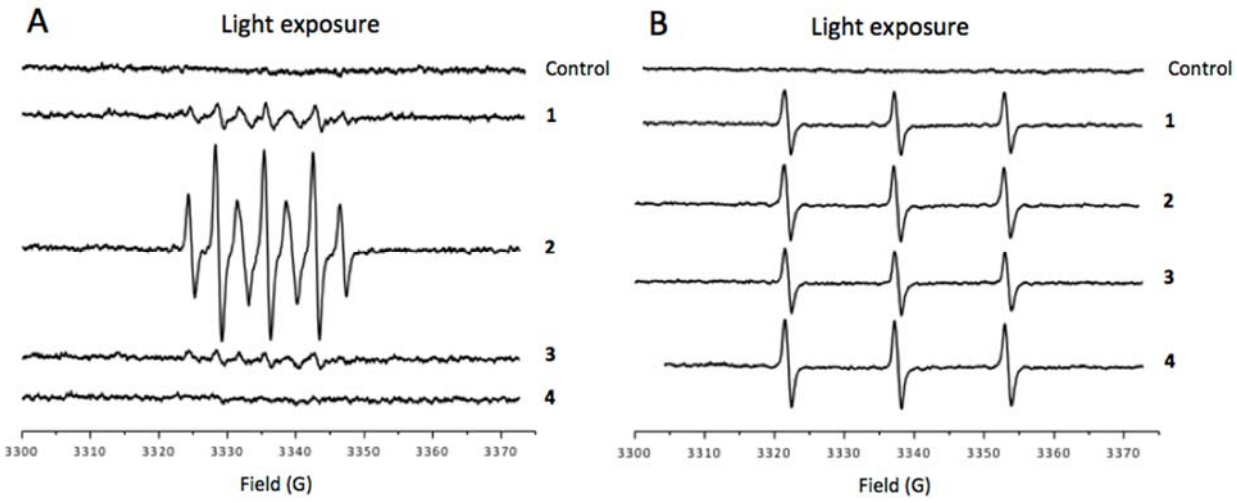
A
Light exposure
Control
1
2
3
4
3300
3310
3320
3330
3340
3350
3360
3370
Field (G)
B
Light exposure
Control
1
2
3
4
3300
3310
3320
3330
3340
3350
3360
3370
Field (G)

Fig. 4

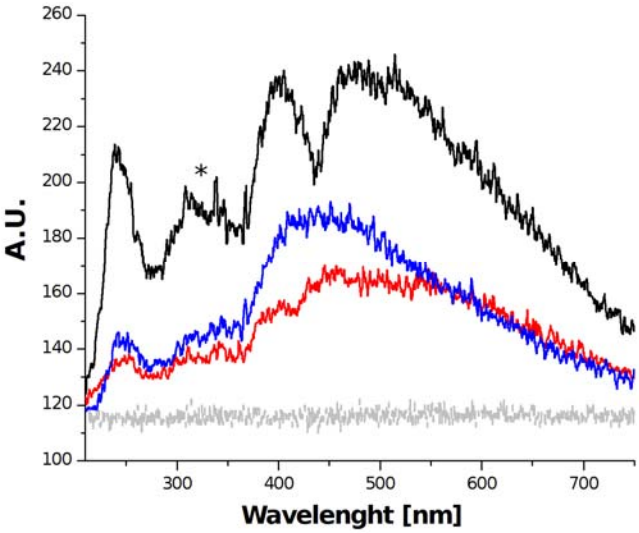
260
240
220
200
180
160
140
120
100
A.U.
*
300
400
500
600
700
Wavelenght [nm]

Fig. 5

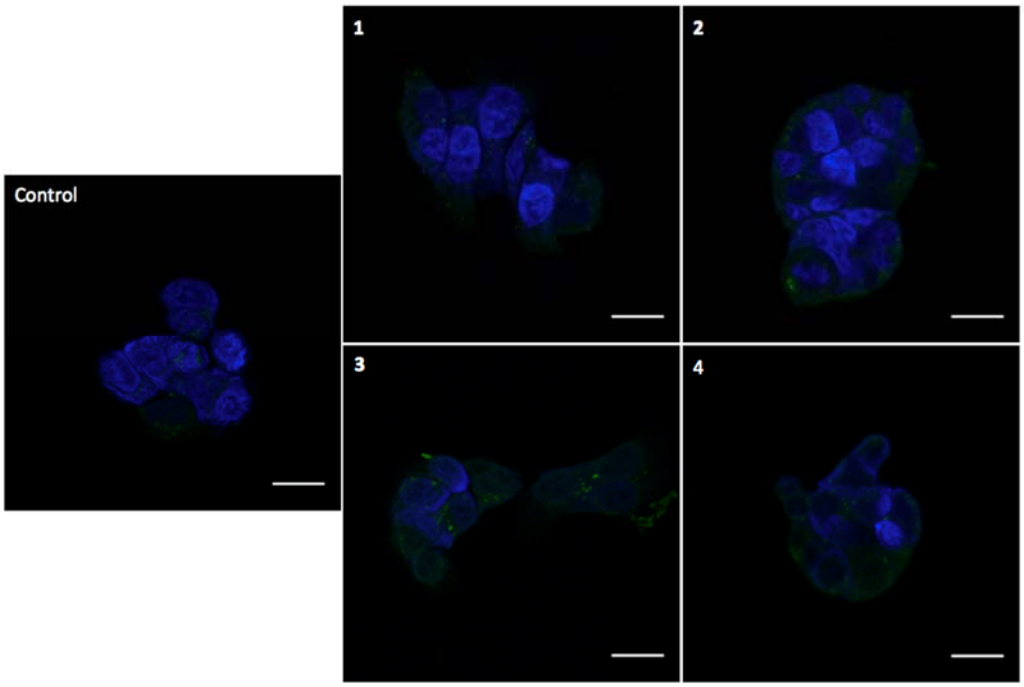

Fig. 6

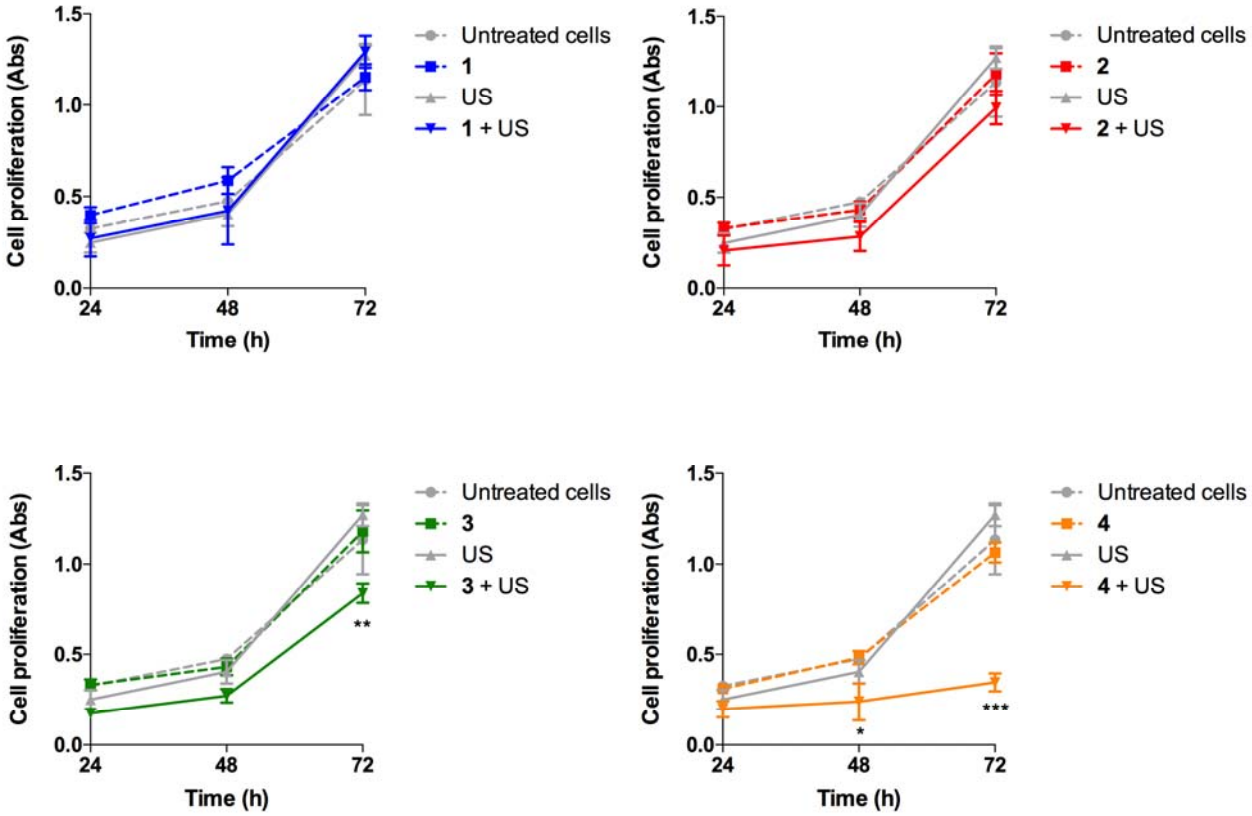
Cell proliferation (Abs)
1.5
1.0
0.5
0.0
24
48
72
Time (h)
Untreated cells
1
US
1 + US
Cell proliferation (Abs)
1.5
1.0
0.5
0.0
24
48
72
Time (h)
Untreated cells
2
US
2 + US
Cell proliferation (Abs)
1.5
1.0
0.5
0.0
24
48
72
Time (h)
**
Untreated cells
3
US
3 + US
Cell proliferation (Abs)
1.5
1.0
0.5
0.0
24
48
72
Time (h)
*
***
Untreated cells
4
US
4 + US

Fig. 7

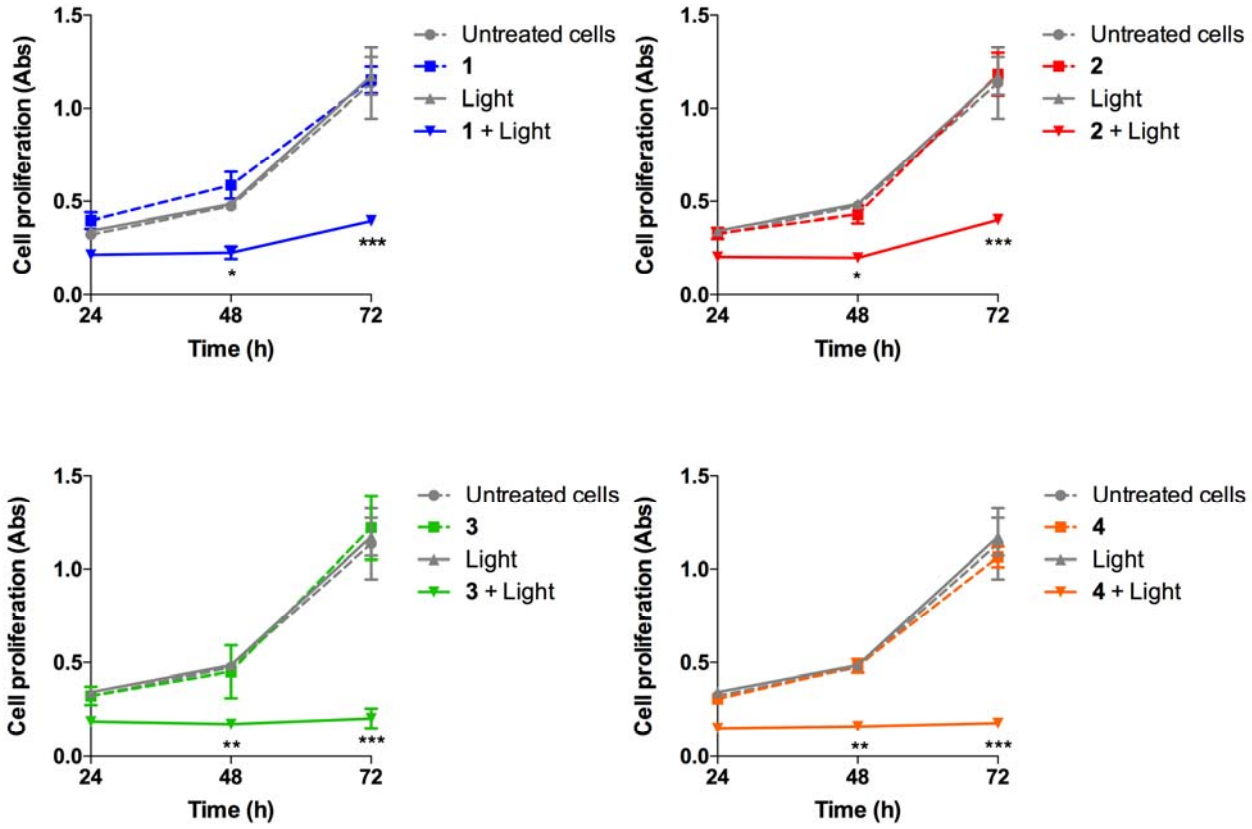
Cell proliferation (Abs)
1.5
1.0
0.5
0.0
24
48
72
Time (h)
Untreated cells
1
Light
1 + Light
*
***
Cell proliferation (Abs)
1.5
1.0
0.5
0.0
24
48
72
Time (h)
Untreated cells
2
Light
2 + Light
*
***
Cell proliferation (Abs)
1.5
1.0
0.5
0.0
24
48
72
Time (h)
Untreated cells
3
Light
3 + Light
**
***
Cell proliferation (Abs)
1.5
1.0
0.5
0.0
24
48
72
Time (h)
Untreated cells
4
Light
4 + Light
**
***

Fig. 8

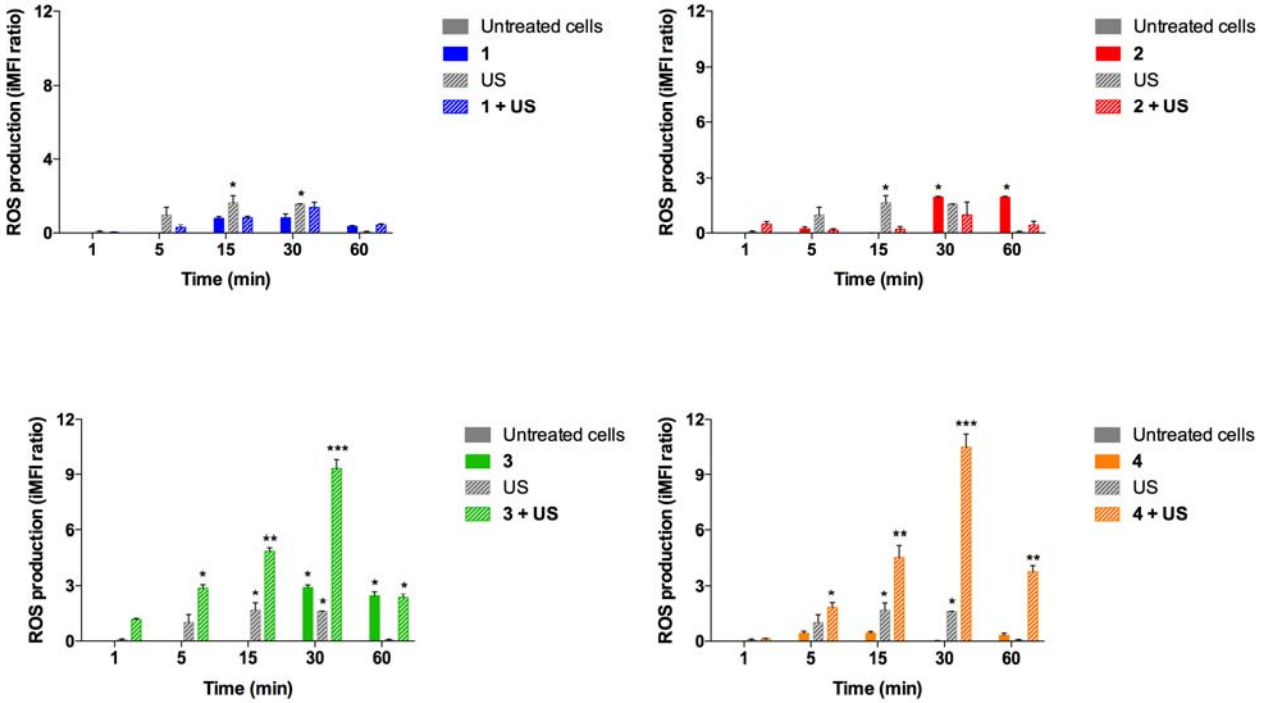
ROS production (iMFI ratio)
Time (min)
Untreated cells
1
US
1 + US
2
2 + US
3
3 + US
4
4 + US

Fig. 9

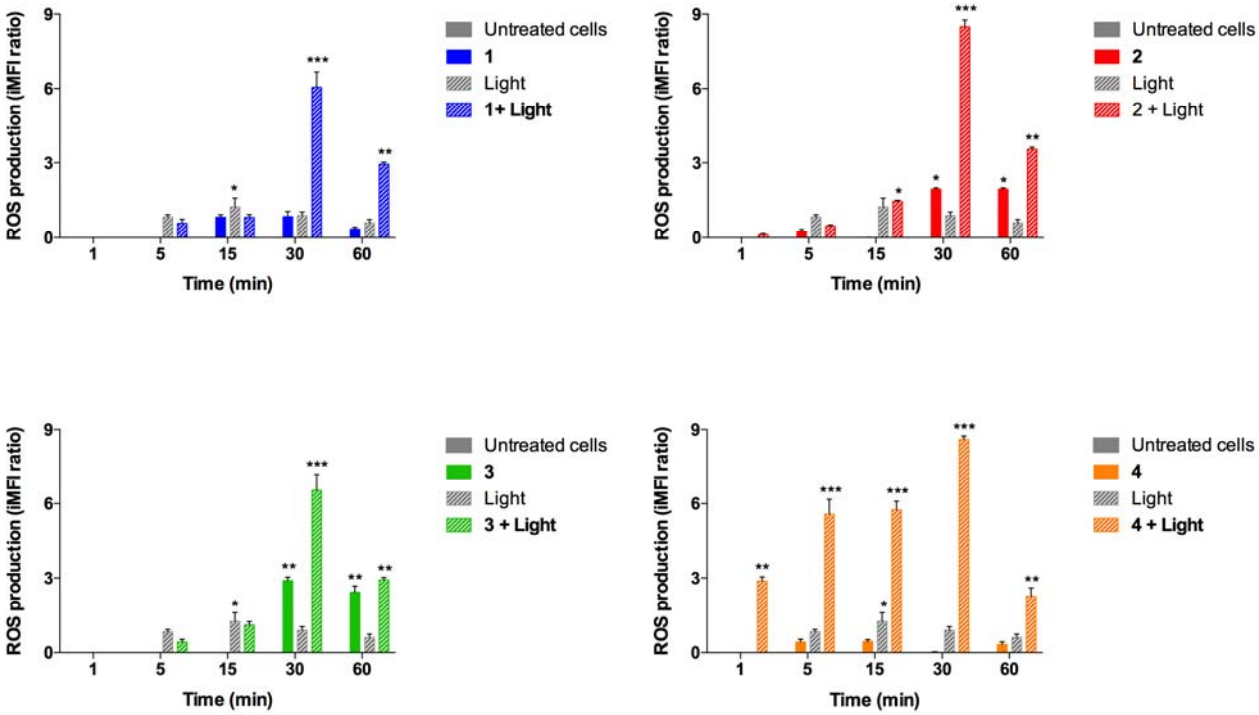
ROS production (iMFI ratio)
Time (min)
Untreated cells
1
Light
1+ Light
2
2 + Light
3
3 + Light
4
4 + Light

Fig. 10

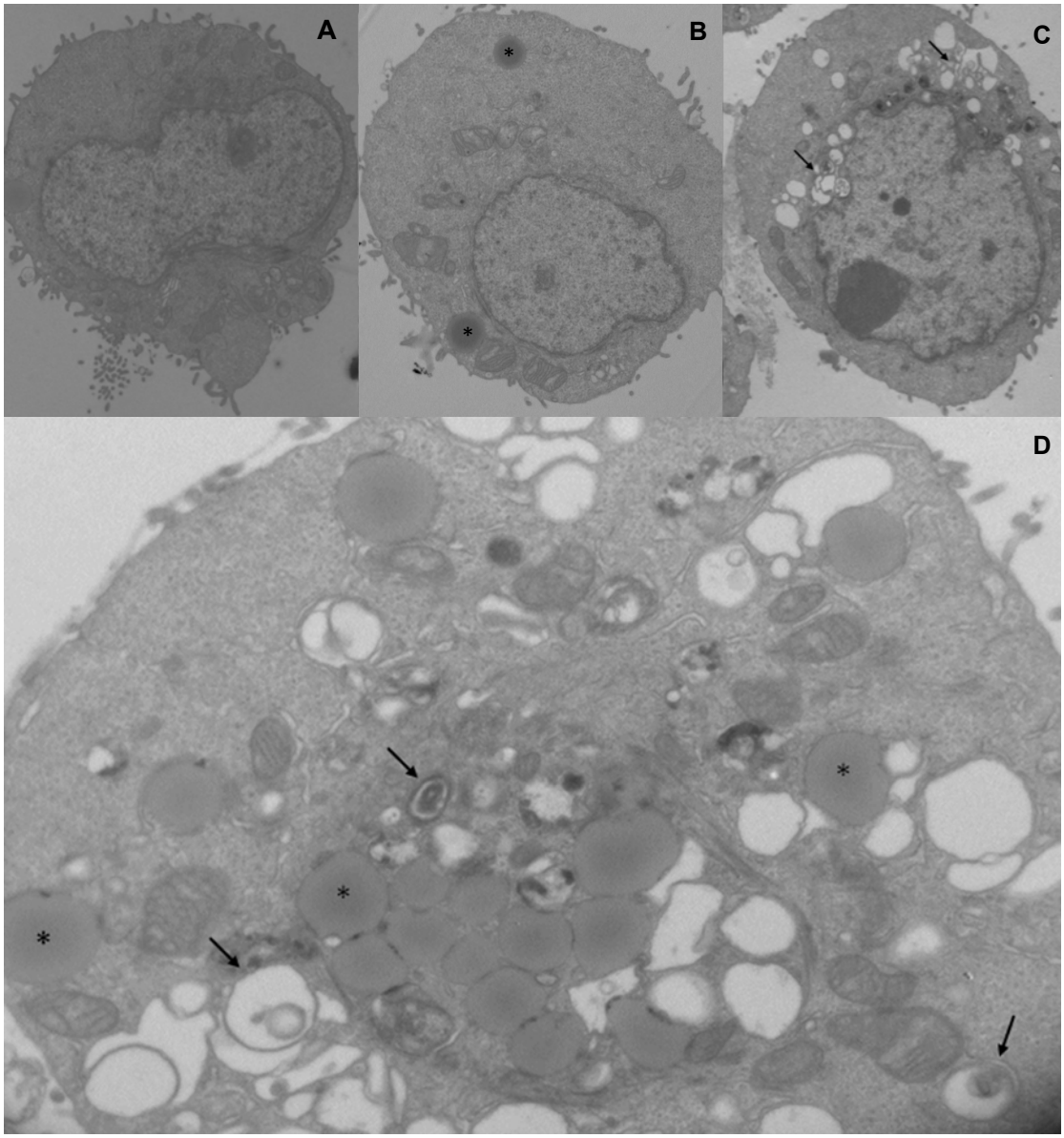

SUPPORTING MATERIALS

A

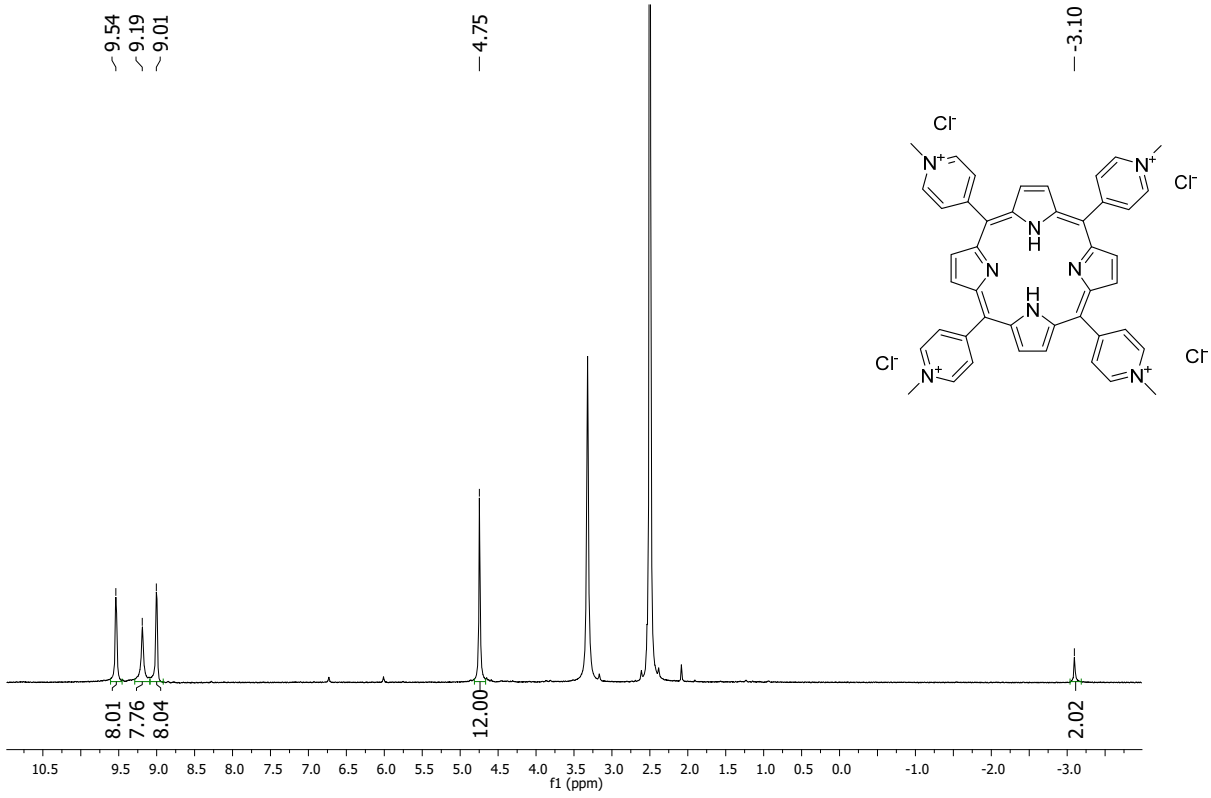

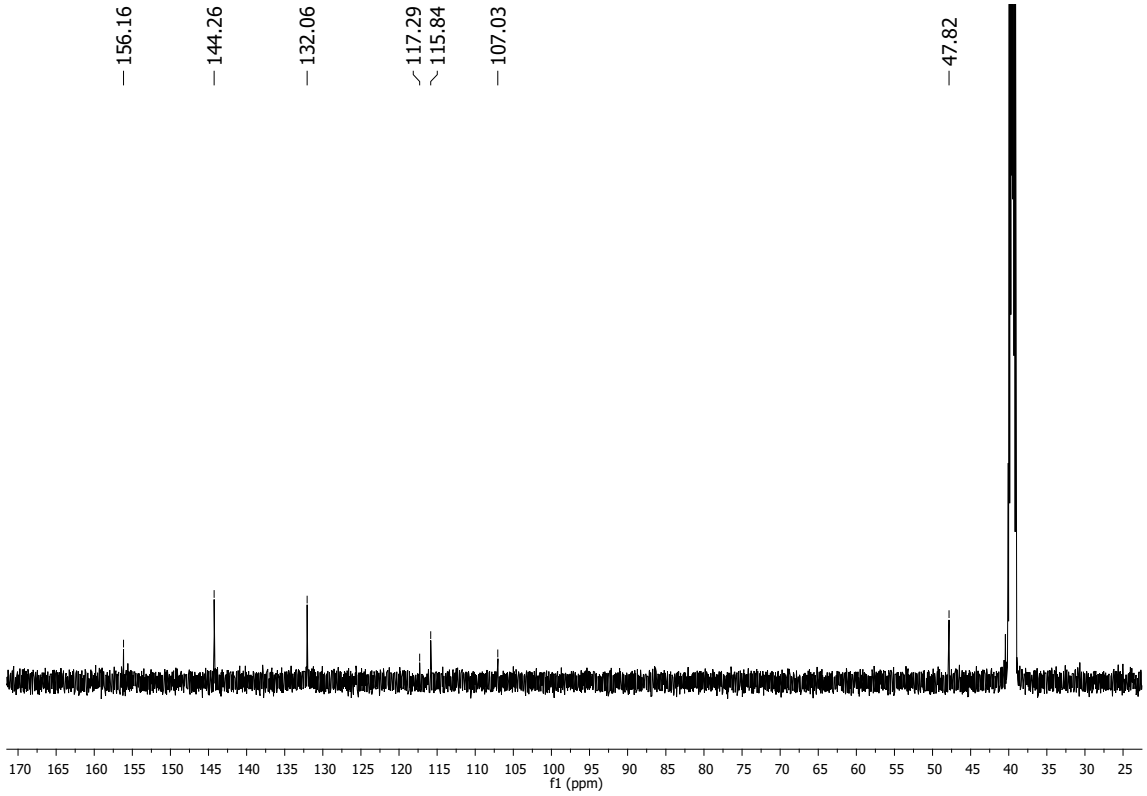

B

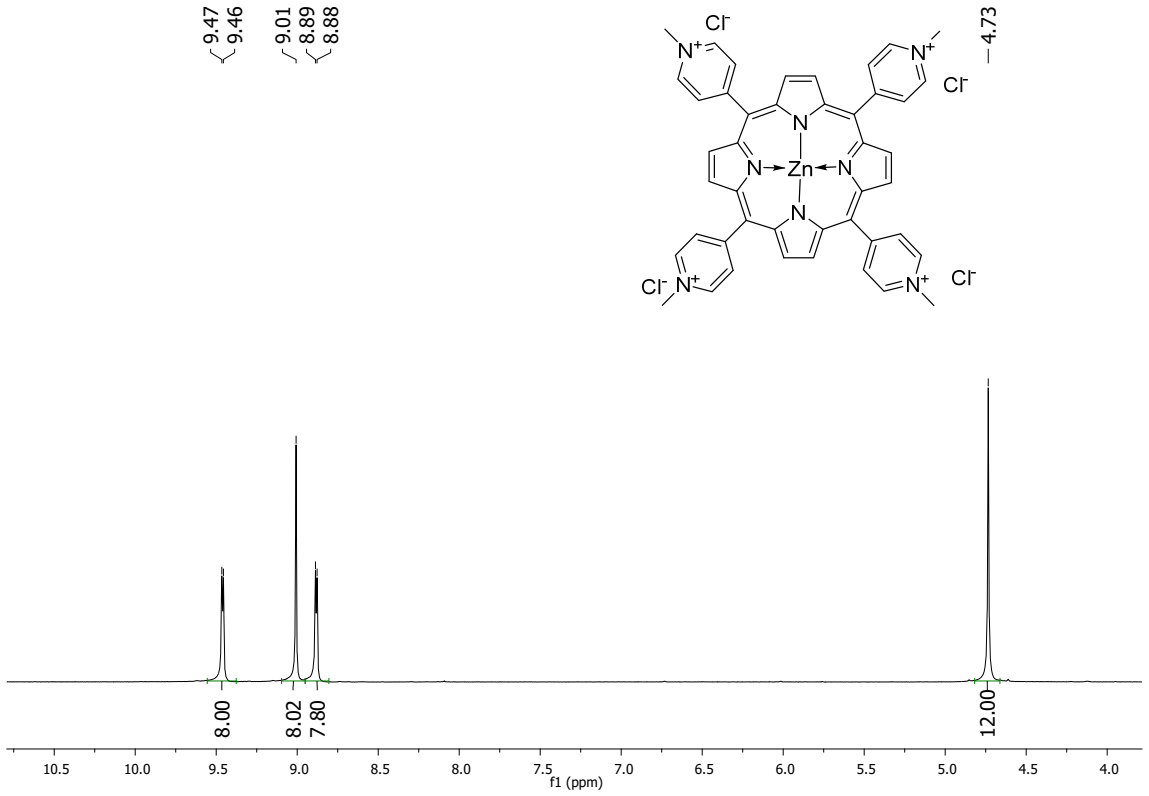
9.47
9.46
9.01
8.89
8.88
4.73
Cl-
N+
Zn
8.00
8.02
7.80
12.00
f1 (ppm)

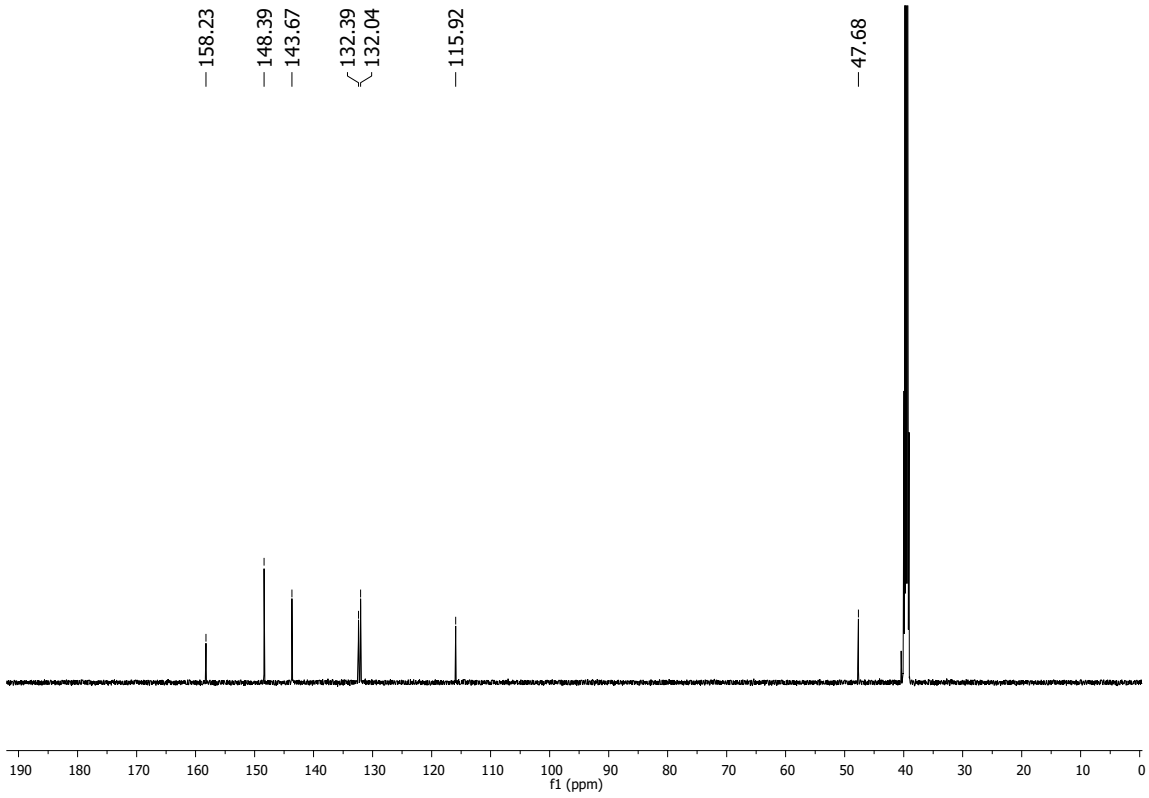
158.23
148.39
143.67
132.39
132.04
115.92
47.68
f1 (ppm)

C

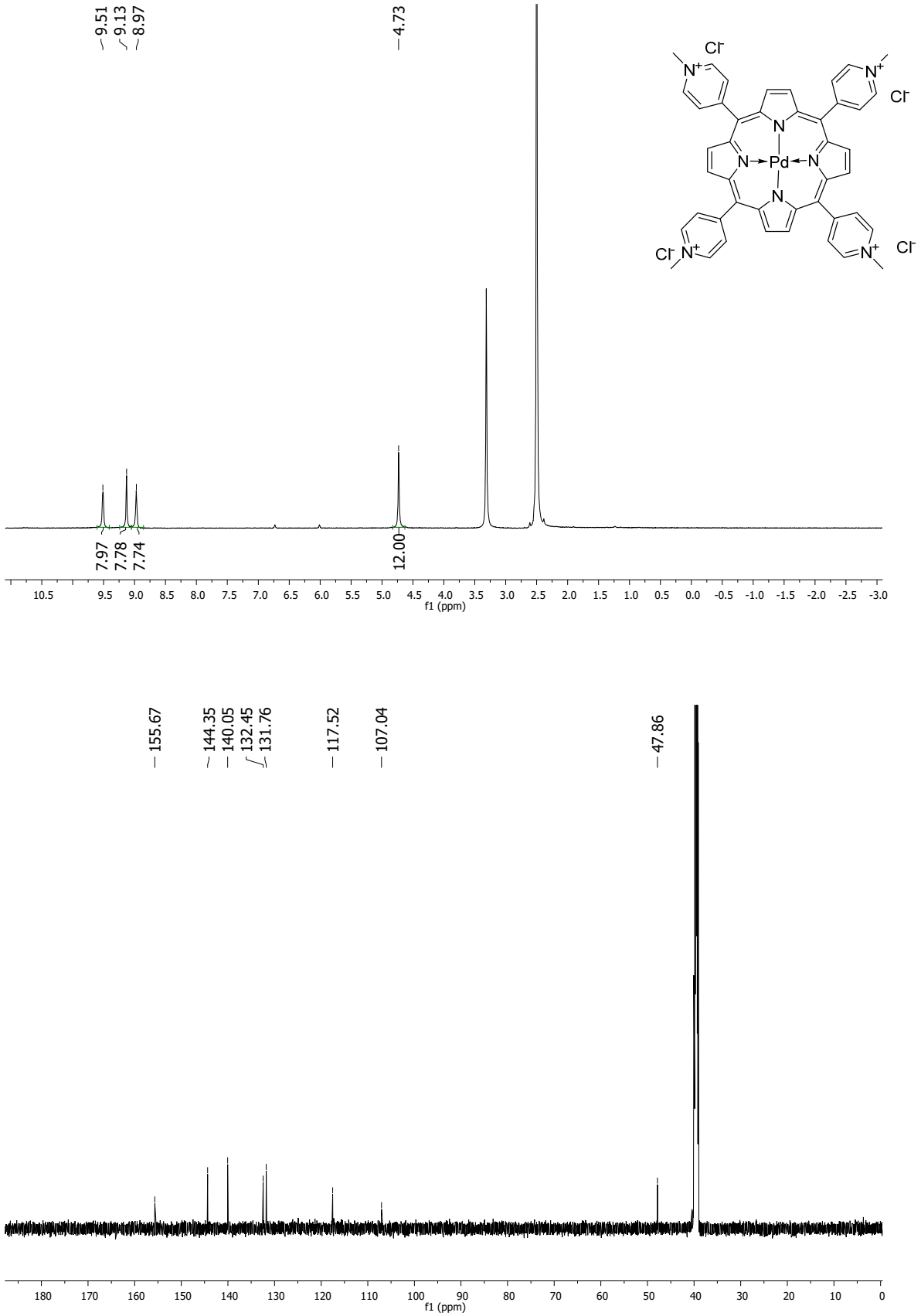

Fig. S1 NMR spectra of porphyrin **1** (A), **3** (B) and **4** (C).

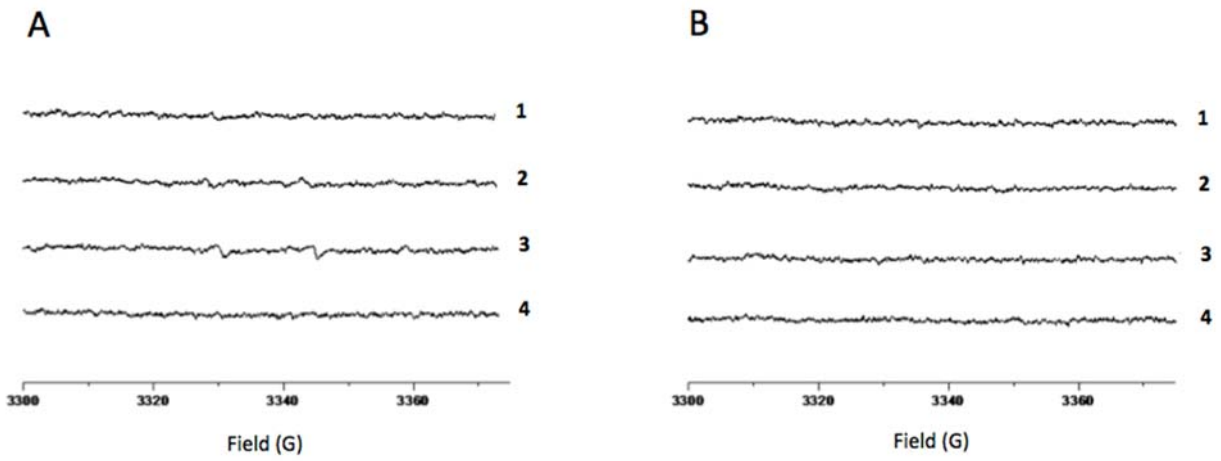

Fig. S2 Generation of A) hydroxyl radicals and B) of singlet oxygen by the various porphyrins (**1**-**4**) detected by EPR spectroscopy in the absence of activation.

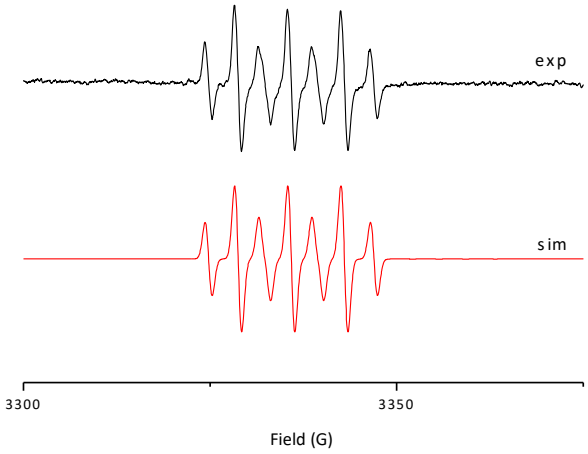

Fig. S3 Simulation of the EPR spectra 2 in figure 3A. Splitting constants, A^H: 3.9 G, A^H: 3.9 G; A^N 7.1 G.

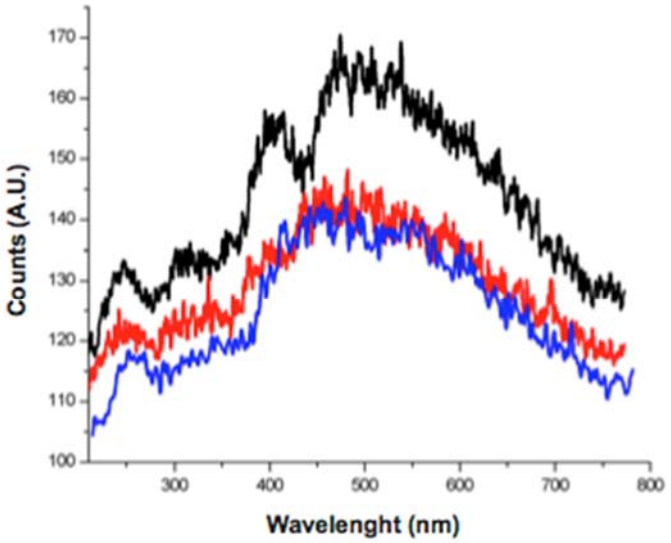

Fig. S4 SL emission spectra of Zn (black) and Pd (red) porphyrin solutions under air saturation during US irradiation at 1.866 MHz. The blue curve refers to multi bubble sonoluminescence (MBSL) recorded in PBS solution. Is possible to note that for black curve the tiny but still detectable, emission from OH radical around 310 nm.

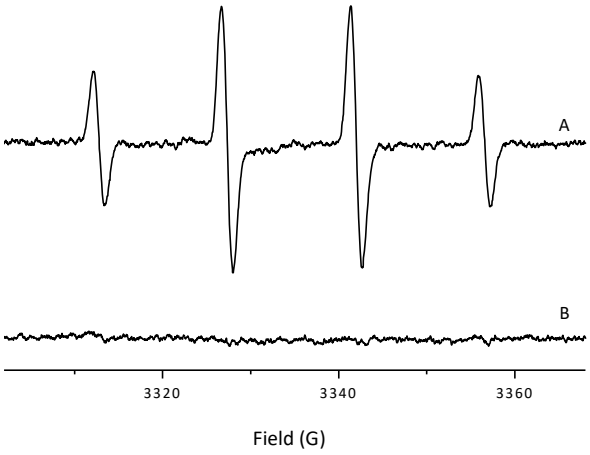

Fig. S5 Generation of hydroxyl radicals by porphyrin 3 in solution (A) and in the same solution after removing oxygen by fluxing with Ar (B).

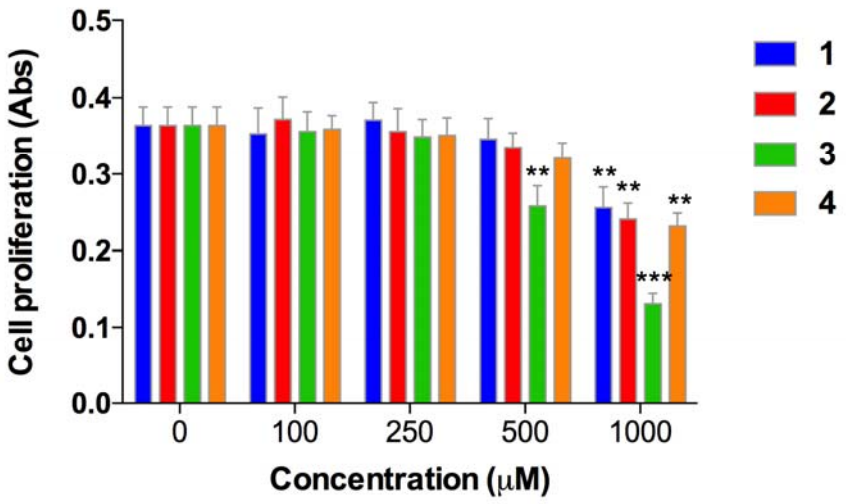

Fig. S6 Effects of porphyrins on HT-29 cell growth. HT-29 cells were incubated for 24 h with increasing concentration of porphyrin **1, 2, 3** and **4** (125, 250, 500 and 1000 μM). Cell proliferation was evaluated after 24 h by WST-1 assay. Statistically significant difference versus untreated cells: ** $p < 0.01$ and *** $p < 0.001$.

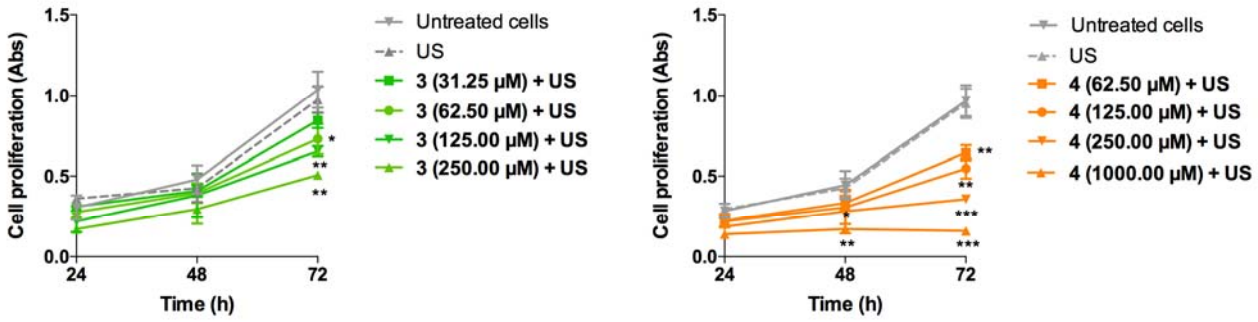

Fig. S7 Effects of sonodynamic treatment on HT-29 cells as a function of sonosensitizer dose. HT-29 cells were incubated for 24 h with increasing concentration of porphyrin **3** (31.25, 62.50, 125.00 and 250.00 µM) and **4** (62.50, 125.00, 250.00 and 500.00 µM)**,** and then exposed to US power at 1.5 W/cm^2 for 5 min at 1.866 MHz. Cell proliferation was evaluated after 24, 48 and 72 h by WST-1 assay. Statistically significant difference versus untreated cells: * $p < 0.05$, ** $p < 0.01$ and *** $p < 0.001$.

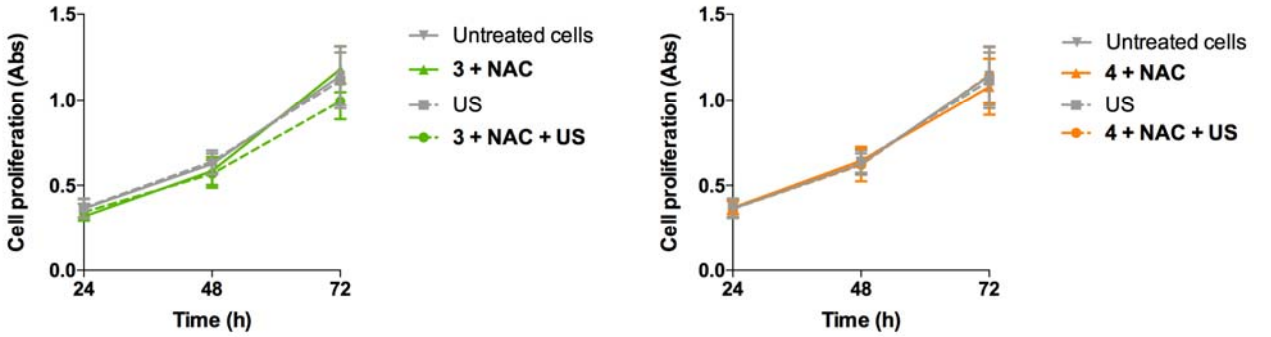

Fig. S8 Effects of sonodynamic treatment on HT-29 cells in presence of the ROS scavenger, N-acvetyl-cysteine (NAC). HT-29 cells were incubated for 24 h with porphyrin **3** at 250 μM and **4** at 500 μM, and 5.0 mM NAC was added for the last 3 h of porphyrins incubation. Cells were then exposed to US power at 1.5 W/cm^2 for 5 min at 1.866 MHz. Cell proliferation was evaluated after 24, 48 and 72 h by WST-1 assay.

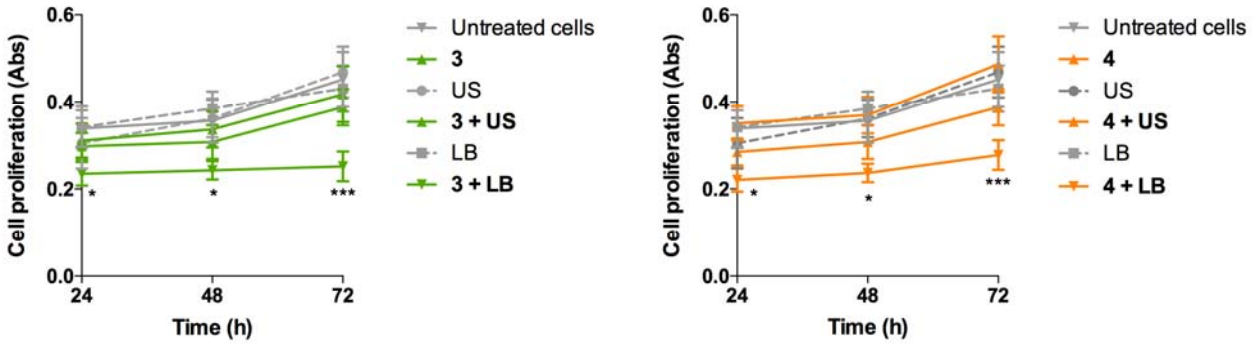

Fig. S9 Effects of sonodynamic and photodynamic treatment on HDF cell growth. HDF cells were incubated for 24 h with porphyrin **3** at 250 μM and **4** at 500 μM, and then exposed to US power at 1.5 W/cm^2 for 5 min at 1.866 MHz and light power at 51.8 mW/cm^2 for 5 min at 400-1050 nm. Cell proliferation was evaluated after 24, 48 and 72 h by WST-1 assay. Statistically significant difference versus untreated cells: * $p < 0.05$, *** $p < 0.001$.